

Nanomanufacturing with DNA Origami: Factors Affecting the Kinetics and Yield of Qdot Binding

By *Seung Hyeon Ko, Gregg M. Gallatin, and J. Alexander Liddle**

[*] Dr. J. A. Liddle. Corresponding-Author, Dr. G. M. Gallatin
Center for Nanoscale Science and Technology, National Institute of Standards and Technology
Gaithersburg, MD 20899.

E-mail: (liddle@nist.gov)

Dr. S. H. Ko

Center for Nanoscale Science and Technology, National Institute of Standards and Technology
Gaithersburg, MD 20899.

Institute for Research in Electronics and Applied Physics, University of Maryland

College Park, MD 20742.

Keywords: (Self-assembly, DNA origami, Nanopatterns, Quantum dot, Binding kinetics)

(Molecularly directed self-assembly has the potential to become a nanomanufacturing technology if the critical factors governing the kinetics and yield of defect free self-assembled structures can be understood and controlled. Here we quantitatively evaluate the kinetics of streptavidin-functionalized quantum dots binding to biotinylated DNA origami and show to what extent the reaction rate and binding efficiency are controlled by the valency of the binding location, the biotin linker length, and the organization and spacing of the binding locations on the DNA. Yield improvement is systematically determined as a function of the valency of the binding locations and as a function of the quantum dot spacing. In addition, the kinetic studies show that the binding rate increases with increasing linker length, but that the yield saturates at the same level for long incubation times. The forward and backward reaction rate coefficients have been determined using a nonlinear least squares fit to the measured binding kinetics, providing considerable physical insight into the factors governing this type of self-assembly process. We find that the value of the dissociation constant, K_d , for the DNA-nanoparticle

complex considered here is up to 7 orders of magnitude larger than that of the native biotin-streptavidin complex. We attribute this difference to the combined effect the much larger size of the DNA origami and the quantum dot have on the translational and rotational diffusion constants.)

1. Introduction

DNA generates molecularly precise nanostructures^[1] that can serve as templates for the hierarchical assembly of additional nanoscale components^[2,3] into more complex, functional devices. DNA origami^[4] is a particularly attractive vehicle for this purpose, being readily configurable into different geometries and easily functionalized to provide a diverse set of binding sites. Origami can themselves be assembled into larger structures^[5-7] and precisely located on templating surface^[8] to create more extended devices or arrays of devices. Finally, they have the potential to be synthesized in large quantities using simple, solution-based methods at room temperature. All of these factors suggest that DNA origami may be a viable nanomanufacturing platform. As a result, there has been intense activity in this area and a number of methods have been developed, using DNA origami-nanoparticle conjugates, to construct a variety of nanoarchitectures.^[9-16] Despite the variety of structures being fabricated, there appear to be common issues related with the poor yields. In this work we therefore seek to explore and understand the factors that control the kinetics and the yield. One common method is to use DNA hybridization to attach nanoparticles (NPs) to origami templates, which, although attractive because it provides site specificity, has resulted in poor yields of the desired NP-DNA conjugates.^[12] Yields can be improved by incorporating multiple interaction sites at a given attachment location, but the absolute yields remain low.^[9,13,15,16] In order to achieve reproducibly

high yields of precisely constructed nanoarchitectures it is important to understand quantitatively the interplay of the diverse factors that affect the binding of nanoparticles to DNA origami. This can be effected by developing metrics to determine the strength and number of binding sites, the optimal linker length, and the minimum binding location separation at a given attachment location necessary to meet a specific yield target.

In this work, the necessary metrics are developed by applying statistical methods to kinetic data for binding of streptavidin-functionalized quantum dots (Qdots) to biotinylated DNA origami. Binding probabilities as a function of time are extracted from atomic force microscope (AFM) images, and are then used to determine the extent to which linker length, binding site valency, and binding site separation affect the formation of complex nanostructures.

Of particular note, we find that the dissociation constant of the biotinylated DNA origami:streptavidin-Qdot complex is orders of magnitude larger than that reported for the free biotin-streptavidin complex – a result we attribute to differences in the translational and rotational diffusion constants between the two systems.

2. Results and Discussion

2.1. Formation of Qdot-nanopatterns

2.1.1. Choice of binding partners

We chose the binding of streptavidin-functionalized Qdots to biotinylated sites on DNA as a model system because the streptavidin-biotin interaction is strong, generally applicable and well-studied.^[17-20] Streptavidin is a tetrameric protein that binds biotin in solution with extraordinarily high affinity ($K_d = 10^{-15}$ mol L⁻¹),^[20] as compared to, for example, duplex DNA which has a K_d of 6.7×10^{-10} mol L⁻¹ for a 10-mer with 1 mol L⁻¹ NaCl at ≈ 30 °C.^[21] A degree of freedom is

provided by varying the number of biotins at each binding location on the DNA . Each Qdot has an approximate diameter of 20 nm and is functionalized with an average of 5 to 10 streptavidins.^[22,23] Such a strong linker system should, in principle, produce intrinsically high yields that allow for the unambiguous separation of affinity from other yield-influencing factors. It also provides the opportunity for investigating the impact of the DNA and Qdots on the stability of the streptavidin-biotin complex because the binding efficiency is decreased when either partner is attached to a larger object.^[24-30]

2.1.2. Design of DNA origami template

To investigate the influence of binding location separation, and hence steric hindrance, on the yield of the Qdot-DNA complex we used a rectangular shaped origami template,^[4] 100 nm × 70 nm, separately synthesizing templates with three different patterns of biotinylated binding locations (**Figure 1**), with spacings of 50 nm (Design I), 35 nm (Design II) and 22 nm (Design III). To test the effect of binding site valency on yield, monovalent and trivalent binding sites were used. In this case, we synthesized two versions of the origami templates described above, with either one or three biotinylated sites at each binding location. These sites were introduced by replacing selected staple strands by 5'-biotin conjugated strands. Trivalent binding locations consist of adjacent biotins arranged on the vertices of an equilateral triangle approximately 5 nm on a side. This spacing is small enough to allow multivalent interactions between a single Qdot and a binding location, but large enough to preclude multivalent interactions with a single streptavidin, since the spacing between the streptavidin binding pockets is only 2 nm.^[17] The sequences of the biotin-conjugated strands are the same as the corresponding unmodified staple strands except that they have an extra spacer of thymines close to the 5'-biotin conjugation. The

spacer length was varied from four thymines (4T) to ten thymines (10T) to explore the influence of spacer length on the kinetics and yield.

We used origami with a staggered merge pattern, so that all modifications made to the middle of a staple strand lie on the same face of the lattice.^[4] We used a common protocol to load the origami onto mica substrates and verified that it led to more than 90% of the origami having the conjugated biotins facing up (Supporting Information, Figure S1), consistent with previous observations.^[31-33] We tested the accessibility of the biotinylated sites on the DNA origami by adding streptavidin to single biotin conjugated-DNA origami templates. The specific binding of streptavidin on DNA origami was clearly observed (Figure 2), with high yields and with binding positions consistent with the designed binding locations for all three binding location separations. Consistent with a previous report,^[14] the height change that occurred upon streptavidin binding was measured to be $0.67 \text{ nm} \pm 0.16 \text{ nm}$ by cross-section profile analysis of our AFM images (Figure S2).

Qdot nanopatterns on DNA origami were constructed by adding an excess quantity [15:1(Qdot : binding location) molar ratio] of streptavidin-coated CdSe/ZnS core/shell Qdot^[34] directly to origami templates immobilized on a mica surface. Under these conditions, and at room temperature, an incubation time of approximately 15 hours (900 minutes) was sufficient to ensure that equilibrium was reached and was therefore used unless otherwise stated. Designs I and III have four binding locations. Design II has three. The AFM images (Figure 3) clearly show that streptavidin coated-Qdots bind specifically to the biotinylated locations on the templates. As a control, we mixed Qdots with non-biotinylated DNA origami templates and observed no interaction.

2.1.3. Binding efficiency

In order to generate the data for quantitative analysis, we first determined the binding frequency for each design by manually counting the number of Qdots bound to each origami in each AFM image. The frequency with which origami with 0, 1, 2, 3 or 4 occupied sites occur is then used to calculate the probability of occupation, or the binding efficiency, p_{occ} , for a single site by fitting the data to a binomial distribution.

2.2. Trivalent vs monovalent interaction

To assess the effect of trivalent (3B) versus monovalent (1B) binding locations on the yield of bound Qdots, we use a quantitative comparison of yield distribution data for the three different designs, shown in Figure 4, (additional AFM images of larger areas for each case are provided in the Supporting Information, Figures S6, S7, & S8). For Design I, the yield of the desired tetramer pattern increased from $22.1 \% \pm 6.5 \%$ (mean $\pm 1\sigma$) for the monovalent case to $90.2 \% \pm 3.3 \%$ for the trivalent case. The probability of occupation for a single site or the binding efficiency, p_{occ} , increased from $70.0 \% \pm 1.6 \%$ for the monovalent case to $97.6 \% \pm 0.8 \%$ for the trivalent case (Figure S3). For Design II (Figure 4), the desired trimer pattern predominated ($54.3 \% \pm 6.1 \%$) for the 3B-DNA origami whereas the 1B-DNA origami produced mainly dimers ($47.9 \% \pm 8.7 \%$). Similarly, Design III (Figure 4) generated $19.5 \% \pm 4.9 \%$ of the designed tetramer Qdot pattern for the 3B-DNA origami, while more than 90 % of the corresponding 1B-DNA origami had only monomer or dimer patterns. The calculated p_{occ} for 3B-origami was $81.8 \% \pm 2.6 \%$ for Design II, falling to $71.5 \% \pm 2.0 \%$ for Design III, while the corresponding 1B-origami templates displayed significantly lower binding efficiencies of $58.2 \% \pm 5.3 \%$ for Design II and $40.0 \% \pm 1.4 \%$ for Design III. As expected, increasing the number of

binding sites at a binding location leads to higher yields. We attribute this improvement to both the increased binding probability offered by the effectively larger trivalent binding locations, as well as to the possibility of multiple biotin interactions with the same Qdot. However, as we highlight below, increasing binding site valency does not guarantee perfection in the resulting nanostructure.

2.3. Steric Effects

Design I has the largest binding location spacings: 50 nm along the 70 nm side and 65 nm along the 100 nm side of the origami. As discussed above, in the case of trivalent binding locations, a high yield of Qdots bound to each location on a template was observed, generating a rectangular tetramer pattern (Figure 3). The average spacings (mean $\pm 1\sigma$) between Qdots measured from AFM images were $52.7 \text{ nm} \pm 4.3 \text{ nm}$ and $70.1 \text{ nm} \pm 5.9 \text{ nm}$ along the 70 nm and 100 nm sides, respectively. These measurements show good agreement with the design parameters and are consistent with the small displacements observed in the images presented by other workers.^[9,11,14] For Design II (35 nm designed spacing), we observed trimer patterns of Qdots with an average spacing of $40.8 \text{ nm} \pm 6.0 \text{ nm}$, but the Qdots were not always arrayed linearly along the diagonal of the origami. Based on the statistical analysis presented below we believe this is primarily an artifact induced by capillary forces acting during drying. Design III (22 nm designed spacing) generated predominantly trimer Qdot patterns, with Qdot-to-Qdot separations of $42.1 \text{ nm} \pm 5.0 \text{ nm}$ – double the spacing expected for this design. We occasionally observed tetramers with center-to-center distances of $31.7 \text{ nm} \pm 7.2 \text{ nm}$. The extent of the displacements from the designed positions becomes larger as the spacing between binding locations is reduced from Design II to III. In addition, we observe significant and frequent distortions of the origami template occurring for the smallest binding location spacing. In contrast to these observations, as

mentioned above, a control experiment of streptavidin binding to DNA origami templates with singly-biotinylated binding locations showed no significant difference in binding efficiency between the three different designs. In addition, streptavidin was observed to bind with high yield and placement accuracy to all the pre-designed binding locations, even at the smallest spacing (22 nm) in Design III. This result is consistent with the previously reported observations allowing for the differences in experimental conditions and design of binding systems.^[35]

The influence of sterics on binding was quantified by comparing the distribution of bound Qdots against the fit binomial distribution. It should be noted that in all cases the values of p_{occ} computed by fitting to the binomial distribution were virtually identical to the overall percentage of occupied sites, as expected. The binomial distributions computed for Design II using the calculated values of p_{occ} fit the measured data to within the error bars, suggesting that the reduced occupation probability relative to Design I is a result only of a reduction in the binding rate relative to the unbinding rate. However, for Design III it is clear that the binomial distributions computed using the calculated values of p_{occ} do not fit the data which is consistent with the large degree of pattern distortion. The trimer and tetramer states in the 1B-DNA origami and the tetramer state in the 3B-DNA origami are under occupied. This has the effect of pushing the distribution to lower occupancy states since the sum of the percentages of bound Qdots is always 100 %.

The deviation of the site occupation data from the expected distribution, combined with the observed displacement of the bound Qdots from the designed positions for Design III suggest that electrostatic and/or steric effects between neighboring Qdots become significant as the binding location spacing tends towards the size of the Qdots.^[34]

2.4. Binding kinetics

In order to quantitatively determine the reaction rate constants of the Qdot-origami self-assembly process, we measured the binding yield as a function of incubation time. Yield data were collected for the 3B-DNA, Design I. Figure 5 shows histograms of the binding location occupancy per template at different incubation times along with the calculated values of p_{occ} for each. The distribution shifts to higher values with increasing incubation time, peaking at two Qdots per origami after 60 minutes of incubation and rising to an equilibrium value of four dots with $97.6 \% \pm 0.8 \%$ yield after 900 minutes. Again, a fit to the binomial distribution for each sample in the time course showed that, for the trivalent Design I, the binding locations act independently with an equal attachment probability.

Although the binding of native streptavidin and biotin is very efficient and stable,^[17,18] we find that the binding reaction rate decreases significantly if the streptavidin and/or biotin are attached to Qdots and DNA origami respectively. Under similar buffer conditions, the binding of free streptavidin and biotin in solution would be almost complete in less than 1 min, a factor of 1000 times faster. Clearly, the reaction rates for the free species cannot be used to determine appropriate reaction times when these same binding partners are attached to bulky species.

The forward and backward rate constants and their 1σ uncertainties are determined using the best fit p_{occ} data and the 1σ uncertainties in p_{occ} derived from the fit for the binding process, which can be represented as



Here k_f and k_b are the forward and backward rate constants, respectively, and $[Qdot]$, $[DNA]$ and $[Qdot\ DNA]$ represent the concentrations of Qdots, DNA origami and bound species, respectively. Note that k_f has units of $\text{volume} \cdot (\text{mole} \times \text{time})^{-1}$ whereas k_b has units of time^{-1} . In our experiments the initial Qdot concentration is much larger than the initial DNA concentration and so the maximum possible concentration of Qdot-DNA complexes is the same as the initial DNA concentration. Although there is some ambiguity in determining the actual value of the DNA concentration (see Experimental section) the fits of $C(t)$ to the p_{occ} data were found to be insensitive to variations in this parameter. Thus the fraction of bound sites or binding efficiency as a function of time, $p_{occ}(t)$, is given by

$$p_{occ}(t) = \frac{C(t)}{C_{DNA0}} \quad (2)$$

where $C(t)$ is the concentration of bound sites as a function of time t and C_{DNA0} is the initial concentration of DNA. Details of the error analysis are provided in the Supporting information. As a guide to interpreting the results presented below, k_f depends predominantly on the rate with which binding occurs, while k_b depends primarily on the equilibrium value of p_{occ} and is indicative of the strength of the binding.

The forward and backward rate constants for streptavidin binding to 1B-DNA origami templates of Design I were calculated using yield data collected for a sequence of different incubation times (Figure 7). Equilibrium was reached in 3 h with only $\approx 60\%$ of DNA origami containing four bound streptavidins, with a value of p_{occ} of $(89.7 \pm 3.7)\%$. The forward and backward rate constants calculated from these data are $(4.1 \pm 0.3) \times 10^3 \text{ L mol}^{-1} \cdot \text{s}^{-1}$ and $(5.0 \pm 0.4) \times 10^{-5} \text{ s}^{-1}$ respectively, compared to $7 \times 10^7 \text{ L mol}^{-1} \cdot \text{s}^{-1}$ and 10^{-7} s^{-1} for free streptavidin/biotin.^[26]

k_f and k_b differ by factors of $\approx 10^{-4}$ and $\approx 10^2$ respectively. These results from our detailed measurements are consistent with those obtained previously using ensemble techniques.^[24-30] k_b is typically reduced significantly when one of the functional groups on biotin is used to attach the linker, as this reduces its ability to hydrogen bond inside the streptavidin binding pocket.^[28, 37]

The discrepancy in the forward reaction rates can be explained by considering the effect the translational and rotational diffusion coefficients have on reaction rate. The translational diffusion coefficient is inversely proportional to the hydrodynamic radius, R_H , of the object, and the rotational diffusion coefficient is inversely proportional to $(R_H)^3$ according to the Stokes-Einstein and Stokes-Einstein-Debye equations, respectively. The overall dependence of the forward reaction rate on size, which reflects the time needed for collisions to occur and for the correct orientation for binding to be achieved, can therefore be estimated to vary roughly as $(R_H)^{-4}$. If we assume that the reaction rate is dominated by the species that diffuses fastest, then we should expect the forward reaction rate for streptavidin-biotin in solution versus streptavidin-origami to scale as $[(R_H \text{ streptavidin})/(R_H \text{ biotin})]^{-4}$. Biotin has a radius of 0.3 nm and the radius of streptavidin is 3 nm,^[17] so we would expect the reaction rate to be reduced by $\approx 10^{-4}$ for streptavidin binding to biotinylated origami. Similarly, the binding reaction between Qdots and origami must also be considered as one between objects much larger than the functional groups.^[38] In this case, k_f is limited by the kinetics of translational and rotational diffusion of the Qdots and DNA origami: the radius of streptavidin coated-Qdots is ≈ 10 nm^[23] whereas the DNA origami has dimensions of $70 \text{ nm} \times 100 \text{ nm} \times 2 \text{ nm}$. We therefore expect that the forward reaction rate for streptavidin-origami versus Qdot-origami to scale as $[(R_H \text{ Qdot})/(R_H \text{ streptavidin})]^{-4} \approx 10^{-2}$. Our simple estimate agrees well with the values observed for the streptavidin-origami case, but the observed forward rate coefficient for the Qdot-origami case is $(2.7 \pm 0.4) \times 10^3 \text{ L}$

$\text{mol}^{-1}\cdot\text{s}^{-1}$, only a factor of two smaller than the streptavidin case. However, we have not taken into account factors such as the presence of multiple streptavidins on each Qdot or the fact that the tethered biotins can explore interaction space more quickly than the origami as a whole. We note that our measured values are consistent with other observations of binding interactions between streptavidin and biotin functionalized Qdots.^[37]

The observed forward binding rate constant of Qdot-bound streptavidin and 3B-DNA origami- conjugated biotin is $(2.0 \pm 0.1) \times 10^3 \text{ L mol}^{-1}\cdot\text{s}^{-1}$, similar to the 1B case, indicating that the addition of extra binding sites does very little to change the forward reaction rate. However, the backward reaction rate constants are $(1.1 \pm 0.2) \times 10^{-4} \text{ s}^{-1}$ and $(6.0 \pm 0.3) \times 10^{-6} \text{ s}^{-1}$ for the Qdot/1B and Qdot/3B cases respectively. These rates differ by a factor of $\approx 5 \times 10^{-2}$. This difference is matched by the increase in p_{occ} from 70 % to 97 %.

The ratio of the forward and backward rate constants for Designs II and III can be determined from the equilibrium values of p_{occ} and the initial concentration of the DNA, $[DNA]_{init}$. For the process shown in Eq (1) we have at equilibrium

$$\frac{k_b}{k_f} = \frac{15 - p_{occ}}{p_{occ}} \frac{1 - p_{occ}}{p_{occ}} \frac{DNA_{init}}{p_{occ}} \quad (3)$$

The initial DNA concentration was the same in all cases and since p_{occ} is restricted to lie between 0 and 1 the factor $(15 - p_{occ})$ cannot vary significantly and so the ratio k_b/k_f (i.e. K_d) scales predominantly as $(1 - p_{occ})p_{occ}^{-1}$. We therefore use the value of $(1 - p_{occ})p_{occ}^{-1}$ as a scaling factor to compare the effect of the different designs on Qdot binding. The results of this analysis are shown in Table 1.

The value of $(1-p_{occ})p_{occ}^{-1}$ for the monovalent case varies by a small amount for the different designs, changing by a factor of ≈ 2 from Design I to Design II and by a factor of ≈ 4 from Design I to Design III. For the trivalent case, however, $(1-p_{occ})p_{occ}^{-1}$ increases by 10 in going from Design I to Design II and by 20 in going from Design I to Design III. Since we can calculate only how the ratio $k_b k_f^{-1}$ scales for Designs II and III we obviously cannot determine separately how k_b and k_f change relative to Design I. However, for Design II the fact that the binomial fit to the data is within the error bars implies that a single value of p_{occ} and hence single values of k_b and k_f apply in that case. By comparison, we speculate that for Design III a single value of k_f cannot be used because of the strong steric hindrance and/or electrostatic effects discussed above.

2.5. More flexible linkages

As discussed above, the rate of Qdot-origami binding is relatively slow and is, at least in part, controlled by the time it takes for the biotin fixed on the origami and the streptavidin bound to the surface of Qdot to find the correct orientation for interaction.^[17,28] In order to explore this in more detail, we systematically increased the length of the biotin-origami linker from 4 thymines (4T), to 6 thymines (6T), 8 thymines (8T), and 10 thymines (10T) for both the 1B and 3B cases to enable the biotin access to a progressively larger configuration space essentially independently of the motion of the origami to which it is attached. Figure 6b shows the results for the 3B case: the binding equilibrium is reached more rapidly as the linker length is increased, by a factor of ≈ 3.5 and ≈ 7 for the 6T and 8T cases respectively. The same overall trend is observed for the 1B case. While values for k_b vary substantially, the values for K_d are all within a factor of ≈ 2 to 3, suggesting that the primary effect of the longer linker is to increase k_f , with minimal effect on

affinity. As the linker length is increased, however, instances of unwanted binding events, including interactions of multiple origami with single Qdots for the singly-biotinylated designs and multiple Qdots binding to a single binding location in the triply-biotinylated origami appear also to increase (Figure 8). As a result, quantitative analysis of the 10T linker case was not possible. The creation of unwanted side products indicates that increased linker length as a strategy for increasing the reaction rate has limited utility. It may be possible to mitigate this effect by moving the Qdot binding locations away from the corners of the origami, thereby making them less accessible to the linkers on adjacent origami.

3. Conclusions

We have performed a quantitative exploration of the parameters that affect the kinetics and yield of streptavidin-biotin mediated Qdot binding to DNA origami, and have found the following results. First, multivalent binding locations provide a dramatic improvement, increasing the yield from $22.1 \% \pm 6.5 \%$ to $90.2 \% \pm 3.3 \%$ as the valency goes from one biotin per binding location to three biotins per binding location. Second, longer linkers increase the reaction rate, but can lead to poorer quality structures and undesirable side products. Third, steric hindrance effects that lead to poor placement precision extend to approximately twice the hydrodynamic radius of the Qdots, significantly limiting the minimum spacing that can be achieved. Although these findings are for a specific system, they likely apply more broadly to self-assembly processes using DNA as a templating structure.

We have demonstrated a quantitative methodology for the analysis of time course data to extract forward and backward reaction rate coefficients. This provides considerable physical insight into the kinetics of these types of self-assembly processes. The K_d of the DNA-

nanoparticle complex is up to 7 orders of magnitude larger than that of the native biotin-streptavidin complex. This disparity arises from the fact that the combined dependence of the translational and rotational diffusion constants on object radius varies as the inverse fourth power. Thus, a small change in the size of the objects being assembled has a dramatic impact on the forward reaction rates, reflected by the rate with which a given assembly process reaches completion.

Our data therefore suggest that purely diffusion-driven self-assembly methods are likely to be limited in terms of rate and yield as the sizes of the components being assembled increases.

4. Experimental

Materials: A single strand M13mp18 (catalog number: N4040S) was purchased from New England Biolab [22]. All unmodified and biotin labeled staple strands were purchased commercially [22], and used without further purification. The streptavidin modified Qdot solution and all other chemicals were purchased commercially [22].

Self-assembly of DNA origami: Rectangular DNA origami was assembled according to the original design by Rothmund [4]. A long single strand of M13mp18 and stapler strands were mixed at molar ratio of 1:5 in 1x TAE/Mg²⁺ buffer [40 mmol L⁻¹ (mM) tris(hydroxymethyl)aminomethane (tris), 20 mmol L⁻¹ (mM) acetic acid, 2 mmol L⁻¹ (mM) ethylenediaminetetraaceticacid (EDTA), and 12.5 mmol L⁻¹ (mM) magnesium acetate, pH 8.0] and slowly annealed at 1°C min⁻¹ from 95°C to room temperature using a DNA thermal cycler. Excess staple strands were removed by washing four to five times with 1x TAE/Mg²⁺ buffer (400 µL) in a “100 000 molecular weight cutoff filter” (100 kDa MWCO) centrifuge filter at 3500 x g for 2 min in a microcentrifuge. To avoid stacking of origami along vertical edges, staple strands on vertical edges have been omitted.

Preparation and AFM Imaging of Qdot-DNA origami conjugates: DNA origami solution (1.5 nmol L^{-1} , $3 \mu\text{L}$) was loaded on freshly cleaved mica surface and left to adsorb on the surface for $\approx 1 \text{ min}$ and dried by gentle blowing with compressed air. The Qdot solution was added on the origami sample at $15 \times$ molar ratio to the binding locations on an origami and incubated for 15 hr , unless otherwise stated, in a Petri dish with moist wipes at room temperature. After incubation, unbound Qdots were washed away with DI-water and the sample was dried again.

To verify that the procedures to create the conjugates leave a significant fraction of the DNA origami on the mica surface, we calculated the expected number of origami per surface area on the basis of the origami concentration in the applied solution and compared that to our experimental results. A drop of DNA origami solution ($3 \mu\text{L}$) contains roughly 3×10^9 origami. When deposited on mica, this volume makes a spot with a diameter of 0.8 cm to 1 cm . If all of the origami in the drop settle on the mica surface and remain adsorbed after drying, the density of origami should be about $20 \mu\text{m}^{-2}$ to $30 \mu\text{m}^{-2}$. The AFM images usually cover a $9 \mu\text{m}^{-2}$ area, which means that each image should contain about 200 origami. The number of discrete origami detected in each image ranged from 30 to 140, showing that about 10 % to 80 % of the origami remains on the mica surface.

AFM imaging was performed under dry conditions in tapping mode with standard silicon cantilevers (PPP-NCH) with a nominal spring constant of 42 N m^{-1} (range of 10 N m^{-1} to 130 N m^{-1}) and resonance frequency between 204 kHz and 497 kHz [22, 39]. The tip-surface interaction was minimized by optimizing the scan set point. We verified that the AFM imaging process did not perturb the dot-origami complexes by performing repeated scans of the same area, and confirming that the first and last images were effectively identical. To ensure adequate statistics, more than 240 origami were counted in multiple (between 4 and 8) AFM images.

Acknowledgements

(The authors thank Veronika Szalai and Paul W. K. Rothmund for discussions and theoretical insights. The authors also thank Rachel Cannara and Zhao Deng for allowing us to use the AFM.) Supporting Information is available online from Wiley InterScience or from the author.

Received: ((will be filled in by the editorial staff))

Revised: ((will be filled in by the editorial staff))

Published online: ((will be filled in by the editorial staff))

- _ [1] (N. C. Seeman, *Mol. Biotechnol.* **2007**, *37*, 246.)
- _ [2] (T. LaBean, H. Li, *Nanotoday* **2007**, *2*, 26.)
- _ [3] (C. M. Niemeyer, U. Simon, *Eur. J. Inorg. Chem.* **2005**, *2005*, 3641.)
- _ [4] (P.W. K. Rothmund, *Nature* **2006**, *440*, 297.)
- _ [5] (R. D. Barish, R. Schulman, P.W. K. Rothmund, E. Winfree, *Proc. Natl. Acad. Sci. USA.* **2009**, *106*, 6054.)
- _ [6] (W. Liu, H. Zhong, R. Wang, N. Seeman, *Angew. Chem. Int. Ed.* **2011**, *50*, 264.)
- _ [7] (M. Endo, T. Sugita, Y. Katsuda, K. Hidaka, H. Sugiyama, *Chem. Eur. J.* **2010**, *16*, 5362.)
- _ [8] (R. J. Kershner, L. D. Bozano, C. M. Micheel, A. M. Hung, A. R. Fornof, J. N. Cha, C. T. Rettner, M. Bersani, J. Frommer, P. W. K. Rothmund, G. M. Wallraff, *Nature Nanotech.* **2009**, *4*, 557.)
- _ [9] (J. Sharma, R. Chhabra, C. S. Andersen, K. V. Gothelf, H. Yan, Y. Liu, *J. Am. Chem. Soc.* **2008**, *130*, 7820.)
- _ [10] (L. A. Stearns, R. Chhabra, J. Sharma, Y. Liu, W. T. Petuskey, H. Yan, J. C. Chaput, *Angew. Chem. Int. Ed.* **2009**, *48*, 8494.)

- _[11] (A. M. Hung, C. M. Micheel, L. D. Bozano, L. W. Osterbur, G. M. Wallraff, J. N. Cha, *Nature Nanotech.* **2010**, *5*, 121.)
- _[12] (S. Pal, Z. Deng, B. Ding, H. Yan, Y. Liu, *Angew. Chem. Int. Ed.* **2010**, *49*, 2700.)
- _[13] (B. Ding, Z. Deng, H. Yan, S. Cabrini, R. N. Zuckermann, J. Bokor, *J. Am. Chem. Soc.* **2010**, *132*, 3248.)
- _[14] (H. Bui, C. Onodera, C. Kidwell, Y. Tan, E. Graugnard, W. Kuang, J. Lee, W. B. Knowlton, B. Yurke, W. L. Hughes, *Nano Lett.* **2010**, *10*, 3367.)
- _[15] (S. Rinker, Y. Ke, Y. Liu, R. Chhabra, H. Yan, *Nature Nanotech.* **2008**, *3*, 418.)
- _[16] (B. Ding, H. Wu, W. Xu, Z. Zhao, Y. Liu, H. Yu, H. Yan, *Nano Lett.* **2010**, *10*, 5065.)
- _[17] (P. C. Weber, D. H. Ohlendorf, J. J. Wendoloski, F. R. Salemme, *Science* **1989**, *243*, 85.)
- _[18] (A. Chilkoti, P. S. Stayton, *J. Am. Chem. Soc.* **1995**, *117*, 10622.)
- _[19] (M. L. Jones, G. P. Kurzban, *Biochem.* **1995**, *34*, 11750.)
- _[20] (T. Sano, C. R. Cantor, *J. Biol. Chem.* **1990**, *265*, 3369.)
- _[21] (L. E. Morrison, L. M. Stols, *Biochem.* **1993**, *32*, 3095.)
- _[22] (The full description of the procedures used in this paper requires the identification of certain commercial products and their suppliers. The inclusion of such information should in no way be construed as indicating that such products or suppliers are endorsed by NIST or are recommended by NIST or that they are necessarily the best materials, instruments, or suppliers for the purposes described.)
- _[23] (Qdot Streptavidin Conjugates, Molecular Probes, Inc. **2007**, 1.)
- _[24] (T. Buranda, G. P. Lopez, J. Keij, R. Harris, L. A. Sklar, *Cytometry* **1999**, *37*, 21.)
- _[25] (J. A. Thompson, H. H. Bau, *J. Chromatogr. B* **2010**, *878*, 228.)
- _[26] (C. Ku, B. B. Lentricchia, *J. Colloid Int. Sci.* **1989**, *132*, 578.)

- _[27] (D. Eberbeck, C. Bergemann, F. Wiekhorst, U. Steinhoff, L. Trahms, *J. Nanobiotech.* **2008**, *6*, 1.)
- _[28] (T. Buranda, G. M. Jones, J. P. Nolan, J. Keij, G. P. Lopez, L. A. Sklar, *J. Phys. Chem. B* **1999**, *103*, 3399.)
- _[29] (S. Huang, M. D. Stump, R. Weiss, K. D. Caldwell, *Anal. Biochem.* **1996**, *237*, 115.)
- _[30] (S. Zhao, W. M. Reichert, *Langmuir* **1992**, *8*, 2785.)
- _[31] (N.V. Voigt, T. Tórring, A. Rotaru, M. F. Jacobsen, J. B. Ravnsbæk, R. Subramani, W. Mamdouh, J. Kjems, A. Mokhir, F. Besenbacher, K. V. Gothelf, *Nature Nanotech.* **2010**, *5*, 200.)
- _[32] (W. Shen, H. Zhong, D. Neff, M. L. Norton, *J. Am. Chem. Soc.* **2009**, *131*, 6660.)
- _[33] (M. Pilo-Pais, S. Goldberg, E. Samano, T. H. LaBean, G. Finkelstein, *Nano Lett.* **2011**, *11*, 3489.)
- _[34] (Purchased from Invitrogen (Qdot 605 Streptavidin conjugate).)
- _[35] (N. Wu, X. Zhou, D. M. Czajkowsky, M. Ye, D. Zeng, Y. Fu, C. Fan, J. Hu, B. Li, *Nanoscale* **2011**, *3*, 2481.)
- _[36] (J. N. Israelachvili, in *Intermolecular & Surface Forces*, 2nd ed. Academic Press, London, **1991**, Ch.13.)
- _[37] (C. K. Chignell, D. K. Starkweather, B. K. Sinha, *J. Biol. Chem.* **1975**, *250*, 5622.)
- _[38] (J. L. Swift, R. Heuff, D. T. Cramb, *Biophys. J.* **2006**, *90*, 1396.)
- _[39] (Purchased from Nanosensors.)

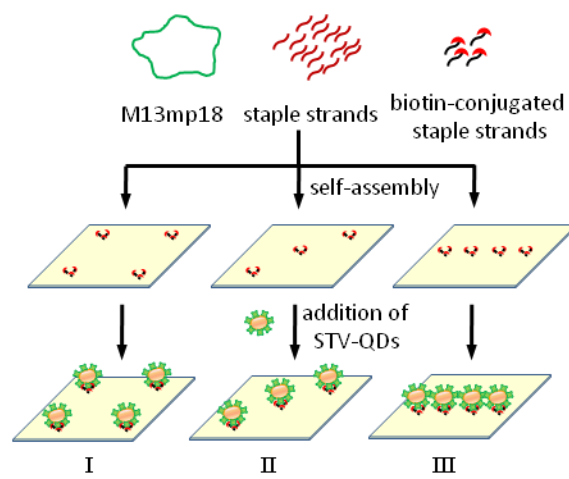


Figure 1. Schematic representation of the fabrication process of Qdot-nanopatterns on DNA origami templates. Groups of three biotin-conjugated staple strands were located at predetermined binding sites to capture streptavidin (STV)-conjugated Qdots (QDs). The distance between adjacent binding sites was 50 nm (I), 35 nm (II), and 22 nm (III).

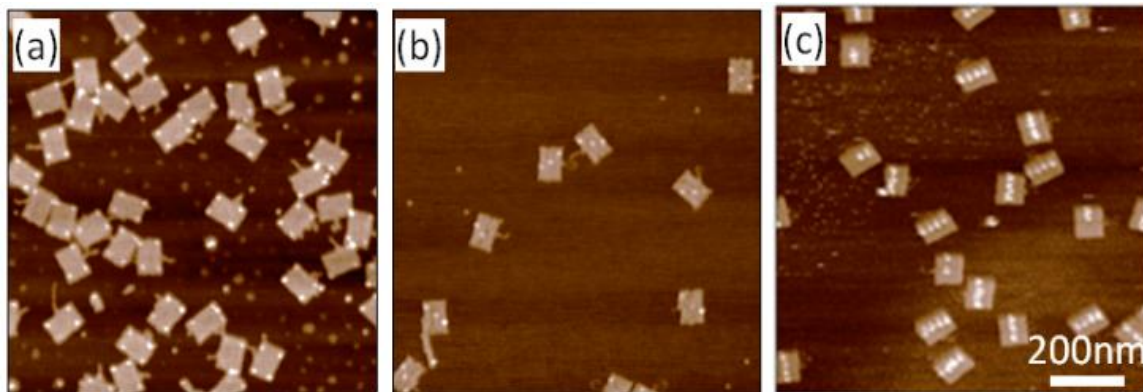


Figure 2. Streptavidin binding on pre-defined singly-biotinylated binding locations on DNA origami template. (a) Design I, (b) Design II, and (c) Design III observed after an incubation time of 180 minutes.

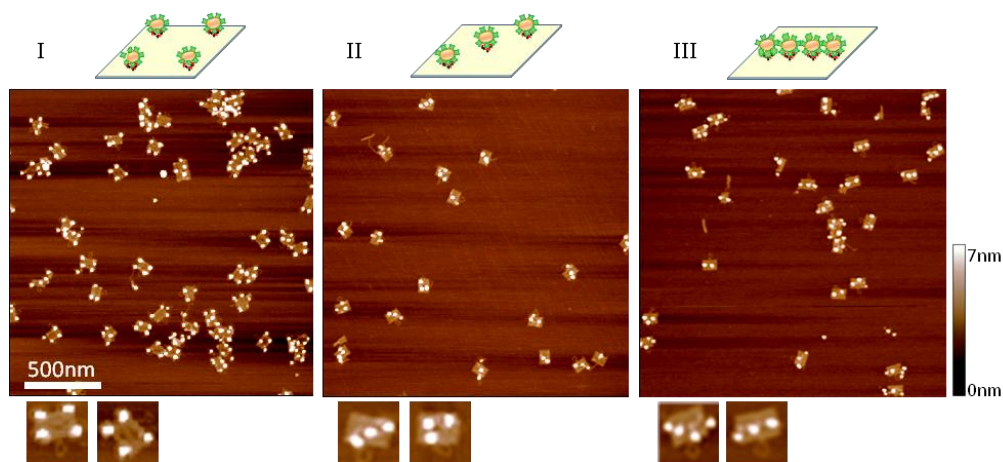


Figure 3. AFM images of Qdot nanopatterns on DNA origami templates containing three biotins per binding location. Three different Qdot nanopatterns (Design I, II, & III) were interrogated. The topographic illustration of each design and its corresponding AFM image are shown. Two magnified images of individual DNA origami are below each larger image.

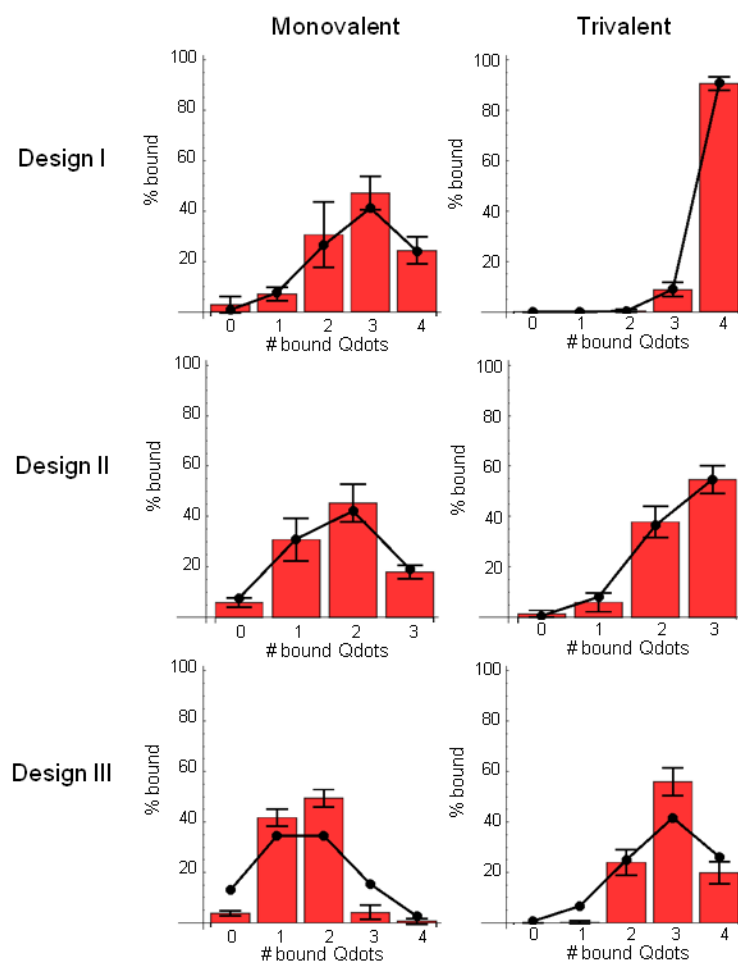


Figure 4. Histogram (bars) for the yield of Qdot-nanopatterns of 1B-origami (Monovalent) and 3B-origami (Trivalent) for Design I, II, and III. Data were collected from AFM images of more than 240 origami pieces for each case. The 1σ variation in the data is shown as error bars. The dots are the binomial distribution for the value of p_{occ} determined by fitting the data. The lines are meant as guide to the eye.

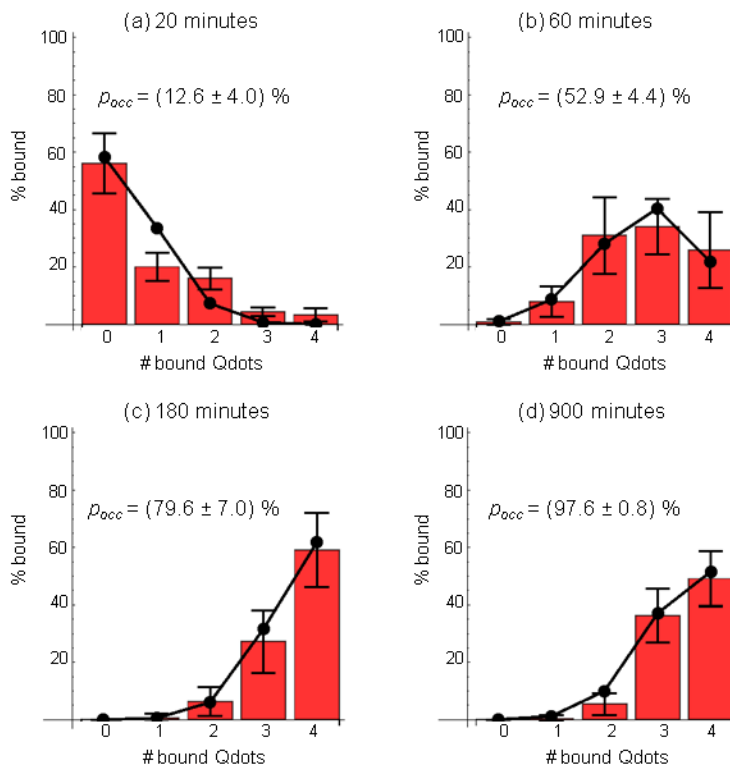


Figure 5. Histogram (bars) for the yield of Qdot patterns generated on 3B-DNA origami of Design I for different incubation times. (a) 20 min, (b) 60 min, (c) 180 min, and (d) 900 min. The mean values of the probability of occupation or binding efficiency, p_{occ} , were calculated using a least squares fit of the averaged data to a binomial distribution. The error bars are the 1σ variation in the results from the separate AFM images for each time. The binomial distributions with these values, p_{occ} (quoted as mean $\pm 1\sigma$) are shown, as a guide to the eye, as solid lines.

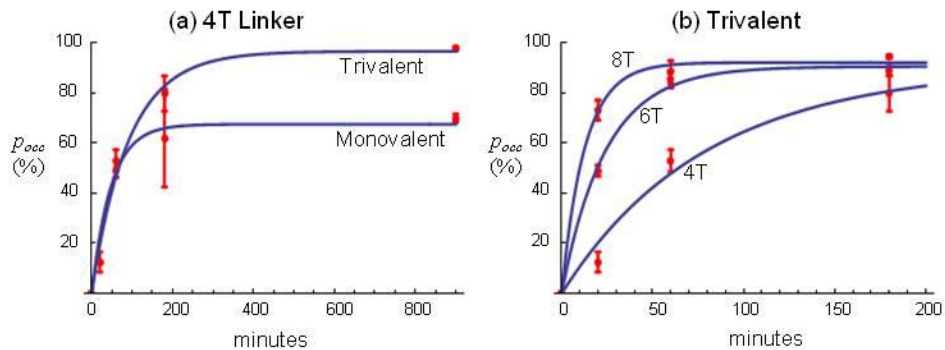


Figure 6. Graphs of p_{occ} as a function of incubation time. (a) The graph shows the 4 thymine (4T) linker case, comparing singly-biotinylated binding locations (monovalent) to triply-biotinylated binding locations (trivalent). In this case the values of the forward reaction rate constant, k_f stays the same but the equilibrium value of p_{occ} is significantly smaller for the single biotin case. (b) The graph shows the trivalent binding location case for three linker lengths, 4 thymine (4T), 6 thymine (6T) and 8 thymine (8T). Increasing the linker length increases k_f without significantly changing the equilibrium value of p_{occ} which is close to 100 % in all cases. The values of k_f and k_b , the backward rate constant, were determined using a least squares fit.

This minimizes $\sum_i (p_{occ,i} - p_{occ})^2$ with respect to k_f and k_b where $p_{occ,i}$ are the measured values of the binding efficiency (red dots) at times t_i and the blue curves are the plots of the function $p_{occ}(t)$ using the fitted values of k_f and k_b . The errors or uncertainties in the values of k_f and k_b were determined by using the least squares equations themselves to determine the sensitivity of k_f and k_b to variations in the measured values of $p_{occ,i}$. These results are discussed in detail in the text.

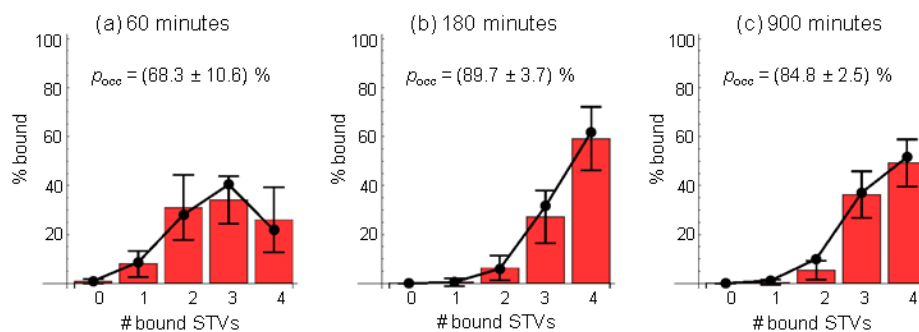


Figure 7. Histogram (bars) for the yield of streptavidin patterns generated on 1B-DNA origami of Design I for different incubation times. (a) 60 min, (b) 180 min, and (c) 900 min. The values of the probability of occupation or binding efficiency, p_{occ} , were calculated using a least squares fit of the data to a binomial distribution. The error bars are the 1σ variation in the results from the separate AFM images for each time, computed using a least squares fit of the data to a binomial distribution. The binomial distributions with these values, p_{occ} (quoted as mean $\pm 1\sigma$) are shown, as a guide to the eye, as solid lines. Equilibrium was reached in 3 hours, the difference between (b) and (c) being within the error bars.

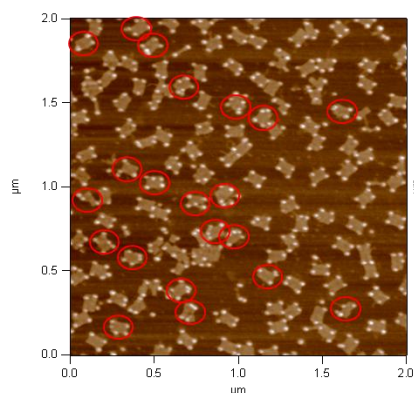


Figure 8. AFM image of quantum dot nanopattern assembled on DNA origami templates with longer linkers after 20 min incubation with 3B-origami of 10T linkers, DNA origami displaying multiple quantum dots at one binding location are highlighted in red.

Table 1. Mean occupation probabilities, p_{occ} , and values of $(1 - p_{occ})p_{occ}^{-1}$ for the monovalent and trivalent versions of Designs I, II and III.

	Monovalent p_{occ} [%]	Monovalent $(1 - p_{occ})p_{occ}^{-1}$	Trivalent p_{occ} [%]	Trivalent $(1 - p_{occ})p_{occ}^{-1}$
Design I	70.0	0.4	97.6	0.02
Design II	58.2	0.7	81.8	0.2
Design III	40.0	1.5	71.5	0.4

The table of contents entry

Nanopatterns of quantum dots are generated on DNA origami at molecular precision. The quantitative studies of their binding kinetics show that the yield can be greatly improved by controlling many factors including the valency of the binding location, the biotin linker length, and the organization and spacing of the binding locations on the DNA.

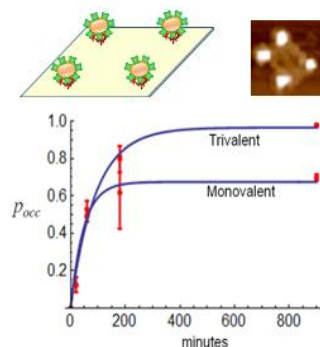
Keyword (Hierarchical Structures, Nanostructures, Quantum Dots, Self-Assembly)

S. H. Ko, G. M. Gallatin, J. A. Liddle*

Nanomanufacturing with DNA Origami: Factors Affecting the Kinetics and Yield of Qdot

Binding

ToC figure



Supporting Information

Nanomanufacturing with DNA Origami: Factors Affecting the Kinetics and Yield of Qdot Binding

By *Seung Hyeon Ko, Gregg M. Gallatin, and J. Alexander Liddle**

[*] Dr. J. A. Liddle. Corresponding-Author, Dr. G. M. Gallatin
Center for Nanoscale Science and Technology, National Institute of Standards and Technology
Gaithersburg, MD 20899.
E-mail: (liddle@nist.gov)
Dr. S. H. Ko
Center for Nanoscale Science and Technology, National Institute of Standards and Technology
Gaithersburg, MD 20899.
Institute for Research in Electronics and Applied Physics, University of Maryland
College Park, MD 20742.

Determination of occupation probability (p_{occ})

For each incubation time, a histogram of the occupancy was fit to a binomial distribution. The values for the probability of occupation, p_{occ} , i.e., the probability that a binding site on DNA origami was occupied by a quantum dot, were computed for each individual AFM image as follows. If N is the number of available binding sites per origami then the probability of finding n bound quantum dots per origami $p(n, p_{occ})$ with $n = 0$ to N is given by

$$p(n, p_{occ}) = \frac{N!}{n! (N-n)!} p_{occ}^n (1-p_{occ})^{N-n} \quad (1)$$

Let d_n be the fraction of DNA origami in the image with n bound quantum dots (Qdots). The best fit value of p_{occ} , in a least squares sense, for the given d_n is found by minimizing $\sum_n d_n - p_n p_{occ}^2$ with respect to p_{occ} . The values of p_{occ} found this way are approximately equal to those obtained simply by counting the total fraction of quantum dot bound sites as expected. The histograms in Figure 4 show the average values of the number of quantum dots bound to a DNA origami at each time. The values of p_{occ} shown in Figure 4 are the average of the best fit values of p_{occ} for the separate AFM images for each time. The error bars are the root mean square (rms) or 1σ variation in these values. The binomial distributions computed from the average p_{occ} values are also shown as connected curves to aid the eye. They fit the data reasonably well in the 20 min, 60 min and 180 min cases and extremely well in the 900 min case, implying that for the trivalent version of Design I the binding locations are acting independently with each having an equal attachment probability.

The best fit value of p_{occ} , and the 1σ uncertainties can be used to determine the forward and backward rate constants and the 1σ uncertainties for the binding/unbinding process which can be represented as



Here k_f and k_b are the forward and backward binding rate constants, respectively. The solution for the concentration of bound sites C_t as a function of time t in terms of the initial concentrations of Qdots and DNA, C_{QD0} and C_{DNA0} is derived below and is given by

$$C(t) = \frac{C^+ C^- (1 - \exp[-(C^+ - C^-) k_f t])}{C^- - C^+ \exp[-(C^+ - C^-) k_f t]} \quad (3)$$

where

$$C^\pm = \frac{k_f C_0 + k_b \pm \sqrt{(k_f C_0 + k_b)^2 - 4k_f^2 C_{DNA0} C_{QD0}}}{2k_f} \quad (4)$$

$$C_0 = C_{DNA0} + C_{QD0}$$

Note that k_f has units of volume/(mole×time) whereas k_b has units of 1/time as required.

In our experiments the initial Qdot concentration is much larger than the initial DNA concentration and so the maximum possible concentration of bound Qdot-DNA is the same as the initial DNA concentration. Thus the fraction of bound sites or binding efficiency as a function of time, $p_{occ}(t)$, is given by

$$p_{occ}(t) = \frac{C(t)}{C_{DNA0}} \quad (6)$$

The values of k_f and k_b were determined using a least squares fit, i.e., minimizing

$$\sum_i (p_{occ,i} - p_{occ}(t_i))^2$$

with respect to k_f and k_b where $p_{occ,i}$ are the measured values of the binding

efficiency at times t_i as shown in Figure 5 and the blue curves are the plots of the function

$p_{occupied}(t)$ using the best fit values of k_f and k_b . The errors or uncertainties in the values of k_f

and k_b were determined by using the least squares equations themselves to determine the linear

sensitivity of k_f and k_b to variations in the measured values of $p_{occ,i}$. Details of the error analysis

are provided below. As a guide to interpreting the results presented, k_f predominantly controls

the speed with which binding occurs, while k_b depends primarily controls the equilibrium value

of p_{occ} . Table S1 gives the values $k_f, k_b, K_d = k_b/k_f$ and p_{occ} at equilibrium for Design I.

Table S1. The calculated constants for monovalent and trivalent template of Design I.

Design I	Monovalent	Trivalent
4T Linker	$k_f = (7.7 \pm 0.4) \times 10^3 \text{ L/mol} \cdot \text{s}$ $k_b = (10 \pm 20) \times 10^{-6} / \text{s}$ $K_d = (11 \pm 14) \times 10^{-9} \text{ mol/L}$ $p_{occ}^{equil} = (0.0 \pm 1.6) \%$	$k_f = (6.0 \pm 0.1) \times 10^3 \text{ L/mol} \cdot \text{s}$ $k_b = (6.1 \pm 0.3) \times 10^{-6} / \text{s}$ $K_d = (6.05 \pm 1.6) \times 10^{-10} \text{ mol/L}$ $p_{occ}^{equil} = (7.5 \pm 0.8) \%$
6T Linker	$k_f = (7.0 \pm 0.5) \times 10^3 \text{ L/mol} \cdot \text{s}$ $k_b = (60 \pm 40) \times 10^{-6} / \text{s}$ $K_d = (1.2 \pm 3.0) \times 10^{-9} \text{ mol/L}$ $p_{occ}^{equil} = (4.8 \pm 4.7) \%$	$k_f = (4.1 \pm 0.2) \times 10^3 \text{ L/mol} \cdot \text{s}$ $k_b = (3 \pm 3) \times 10^{-6} / \text{s}$ $K_d = (8.7 \pm 6.7) \times 10^{-10} \text{ mol/L}$ $p_{occ}^{equil} = (8.7 \pm 1.8) \%$
8T Linker	$k_f = (7 \pm 0.1) \times 10^3 \text{ L/mol} \cdot \text{s}$ $k_b = (280 \pm 210) \times 10^{-6} / \text{s}$ $K_d = (2.5 \pm 3.7) \times 10^{-9} \text{ mol/L}$ $p_{occ}^{equil} = (0.3 \pm 2.8) \%$	$k_f = (3.7 \pm 0.5) \times 10^3 \text{ L/mol} \cdot \text{s}$ $k_b = (00 \pm 10) \times 10^{-6} / \text{s}$ $K_d = (25 \pm 10) \times 10^{-10} \text{ mol/L}$ $p_{occ}^{equil} = (4.4 \pm 0.7) \%$

Reaction Equation Solution

Given the generic reaction



and letting N_a , N_b and N_{ab} be the number of species of a , b , and bound ab pairs respectively we

have

$$\begin{aligned}
\partial_t N_{ab} &= -k_b N_{ab} + k_f N_a N_b \\
\partial_t N_a &= k_b N_{ab} - k_f N_a N_b \\
\partial_t N_b &= k_b N_{ab} - k_f N_a N_b
\end{aligned} \quad (8)$$

Mass conservation implies

$$N_a + N_b + 2N_{ab} = \text{constant} \quad (9)$$

which the above set of equations satisfy.

Subtracting the second and third equations gives

$$\partial_t (N_b - N_a) = 0 \Rightarrow N_b - N_a = C \quad (10)$$

where C is a constant which is given by

$$C = N_b(0) - N_a(0) \quad (11)$$

Adding the first and second equations gives

$$\partial_t (N_{ab} + N_a) = 0 \Rightarrow N_{ab} + N_a = D \quad (12)$$

where D is a constant which since $N_{ab}(0) = 0$ is given by

$$D = N_a(0) \quad (13)$$

Substituting these results into the first equation we have

$$\begin{aligned} \partial_t N_{ab} &= -k_b N_{ab} + k_f (D - N_{ab}) - C + D - N_{ab} \\ &= -k_b N_{ab} + k_f (N_{a0} - N_{ab}) - (N_{b0} - N_{ab}) \end{aligned} \quad (14)$$

This can be converted to the integral equation

$$\int_0^{N_{ab}(t)} \frac{dN_{ab}}{-k_b N_{ab} + k_f (N_{a0} - N_{ab}) - (N_{b0} - N_{ab})} = t \quad (15)$$

Now factor the denominator

$$\begin{aligned} -k_b N_{ab} + k_f (N_{a0} - N_{ab}) - (N_{b0} - N_{ab}) &= k_f N_{ab}^2 - (k_f (N_{a0} + N_{b0}) + k_b) N_{ab} + k_f N_{a0} N_{b0} \\ &= k_f (N_{ab} - N_{ab}^+) (N_{ab} - N_{ab}^-) \end{aligned} \quad (16)$$

where

$$N_{ab}^{\pm} = \frac{k_f (N_{a0} + N_{b0}) + k_b \pm \sqrt{k_f^2 (N_{a0} + N_{b0})^2 + k_b^2 - 4k_f^2 N_{a0} N_{b0}}}{2k_f} \quad (17)$$

The integral in (15) can now be done

$$\begin{aligned}
 \int_0^{N_{ab}^t} \frac{dN_{ab}}{-k_b N_{ab} + k_f \frac{N_{a0} - N_{ab}}{N_{b0} - N_{ab}}} &= \int_0^{N_{ab}^t} \frac{dN_{ab}}{k_f \frac{N_{ab} - N_{ab}^+}{N_{ab} - N_{ab}^-}} \\
 &= \frac{1}{k_f \frac{N_{ab}^+ - N_{ab}^-}{N_{ab} - N_{ab}^-}} \int_0^{N_{ab}^t} dN_{ab} \left(\frac{1}{N_{ab} - N_{ab}^+} - \frac{1}{N_{ab} - N_{ab}^-} \right) \\
 &= \frac{1}{k_f \frac{N_{ab}^+ - N_{ab}^-}{N_{ab} - N_{ab}^-}} \ln \left[\frac{N_{ab}^- \frac{N_{ab}^t}{N_{ab} - N_{ab}^-} - N_{ab}^+}{N_{ab}^+ \frac{N_{ab}^t}{N_{ab} - N_{ab}^+} - N_{ab}^-} \right]
 \end{aligned} \tag{18}$$

Solving for N_{ab}^t gives

$$N_{ab}^t = \frac{N_{ab}^- N_{ab}^+ \frac{1 - \exp\left[\frac{N_{ab}^+ - N_{ab}^-}{k_f} t \right]}{N_{ab}^- - N_{ab}^+ \exp\left[\frac{N_{ab}^+ - N_{ab}^-}{k_f} t \right]} \tag{19}$$

Defining the molar concentration $C_{ab} = N_{ab} / (N_A V)$ where $N_A = 1$ mole and V is the volume of the system gives

$$C_{ab}^t = \frac{C_{ab}^- C_{ab}^+ \frac{1 - \exp\left[\frac{C_{ab}^+ - C_{ab}^-}{N_A V k_f} t \right]}{C_{ab}^- - C_{ab}^+ \exp\left[\frac{C_{ab}^+ - C_{ab}^-}{N_A V k_f} t \right]} \tag{20}$$

Note that whereas k_f has units of per particle per time $N_A V k_f$ has units of L·s/mol since $N_A = 6.023 \times 10^{23}$ and V is volume and so

$$N_A V k_f = \frac{k_f}{\text{mol/L}} \tag{21}$$

Since k_f has units of s^{-1} $N_A V k_f$ has units of L/mol·s which is correct when dealing with concentrations. When dealing with concentrations $N_A V k_f$ is usually just replaced by k_f in units of L/Ms. The parameter k_b does not change in going from number to concentration.

Least Squares Fit and Error Propagation Analysis

The maximum value N_{ab} can take is the smaller of the initial values N_{a0} and N_{b0} . Assume

$N_{b0} < N_{a0}$ then $N_{ab}(t) / N_{b0}$ is the fraction of the total possible number of bound ab pairs

present at time t . Noting explicitly the dependence of $N_{ab}(t)$ on k_f and k_b

$$N_{ab}(k_f, k_b, t) = \frac{N_{ab}^-(k_f, k_b) N_{ab}^+(k_f, k_b) [1 - \exp\left[-\frac{N_{ab}^+(k_f, k_b) - N_{ab}^-(k_f, k_b)}{k_f t}\right]]}{N_{ab}^-(k_f, k_b) - N_{ab}^+(k_f, k_b) \exp\left[-\frac{N_{ab}^+(k_f, k_b) - N_{ab}^-(k_f, k_b)}{k_f t}\right]} \quad (22)$$

we have the fraction of bound ab pairs at time t as a function of k_f and k_b is given by

$$f(k_f, k_b, t) = \frac{N_{ab}(k_f, k_b, t)}{N_{b0}} \quad (23)$$

Given the measured values d_i of the fraction of bound ab pairs at times t_i with $i = 1, 2, \dots, s$

where s is the number of sample times, we can determine the values of k_f and k_b by solving

simultaneously the least squares equations

$$\begin{aligned} \frac{\partial}{\partial k_f} \sum_{i=1}^s [f(k_f, k_b, t_i) - d_i]^2 &= 0 \\ \frac{\partial}{\partial k_b} \sum_{i=1}^s [f(k_f, k_b, t_i) - d_i]^2 &= 0 \end{aligned} \quad (24)$$

for k_f and k_b .

Let $f(k_f, k_b, t_i) \equiv f_i$ and to simplify the notation we do not explicitly indicate the dependence of

f_i on k_f and k_b . Evaluating the derivatives yields

$$\begin{aligned} \sum_{i=1}^s [f_i - d_i] \frac{\partial f_i}{\partial k_f} &= 0 \\ \sum_{i=1}^s [f_i - d_i] \frac{\partial f_i}{\partial k_b} &= 0 \end{aligned} \quad (25)$$

These equations are highly nonlinear and the best way to solve for k_f and k_b is numerically. Next given the solutions for k_f and k_b we need to determine the error or uncertainty in their values given the errors or uncertainties in the data values d_i . There are various ways for determining how the errors or uncertainties propagate from the data d_i to the values of k_f and k_b as determined from the least squares analysis. Here we take the straightforward approach of using the least squares equations themselves to determine the sensitivity of the k_f and k_b values to the values of d_i then using the error or uncertainty in the values of the d_i we can determine the error or uncertainty in the values of k_f and k_b . To do this note that the least squares equations define implicitly the dependence of k_f and k_b on the data d_i .

To simplify the notation we will use $k_f = u_1$ and $k_b = u_2$. Indicating the dependence of f_i on u_n explicitly the least squares equations become

$$\sum_{i=1}^s f_i u - d_i \frac{\partial f_i}{\partial u_n} = 0 \quad (26)$$

where $n=1,2$ refers to the k_f and k_b equation, respectively.

Now, to determine how the u_n depends on d_j take the derivative with respect to d_j and noting that the least squares equations themselves impose a dependence of u_n on d_j . i.e., $u_n = u_n(d)$ we have

$$\begin{aligned} 0 &= \frac{\partial}{\partial d_j} \sum_{i=1}^s f_i - d_i \frac{\partial f_i}{\partial u_n} \\ &= \sum_{m=1}^2 \sum_{i=1}^s \left(\left(\frac{\partial u_m}{\partial d_j} \frac{\partial f_i}{\partial u_m} - \delta_{ij} \right) \frac{\partial f_i}{\partial u_n} + f_i - d_i \frac{\partial u_m}{\partial d_j} \frac{\partial^2 f_i}{\partial u_m \partial u_n} \right) \end{aligned} \quad (27)$$

Rearranging gives

$$\sum_{m=1}^2 \sum_{i=1}^s \left(\frac{\partial f_i}{\partial u_m} \frac{\partial f_i}{\partial u_n} + f_i - d_i \frac{\partial^2 f_i}{\partial u_m \partial u_n} \right) \frac{\partial u_m}{\partial d_j} = \frac{\partial f_j}{\partial u_n} \quad (28)$$

Define

$$M_{nm} = \sum_{i=1}^s \left(\frac{\partial f_i}{\partial u_m} \frac{\partial f_i}{\partial u_n} + f_i - d_i \frac{\partial^2 f_i}{\partial u_m \partial u_n} \right) \quad (29)$$

where all the derivatives of f_i are to be evaluated at the values of u_n given by the solution to the least squares equations. Then we have

$$M_{nm} \left(\frac{\partial u_m}{\partial d_j} \right) = \frac{\partial f_j}{\partial u_n} \quad (30)$$

where repeated indices are summed. Solving for $\partial u_m / \partial d_j$ gives

$$\frac{\partial u_m}{\partial d_j} = M^{-1}{}_{mn} \left(\frac{\partial f_j}{\partial u_n} \right) \quad (31)$$

and so $\delta u_m = \frac{\partial u_m}{\partial d_j} \delta d_j = M^{-1}{}_{mn} \frac{\partial f_j}{\partial u_n} \delta d_j$

The noise in the data is uncorrelated and so

$$\langle \delta d_j \delta d_j \rangle = \sigma_{d_j}^2 \delta_{jj'} \quad (32)$$

where σ_{d_j} is the root-mean-square(rms) error in the d_j value. The mean square error in u_m is then given by

$$\sigma_{um}^2 = \langle \delta u_m^2 \rangle \quad (33)$$

with no sum on m and so

$$\begin{aligned}
\sigma_{k_f}^2 &= \langle \delta u_1^2 \rangle = \sum_{n,n',j} M^{-1}_{1n} \left(\frac{\partial f_j}{\partial u_n} \right) M^{-1}_{1n'} \left(\frac{\partial f_j}{\partial u_{n'}} \right) \sigma_j^2 \\
\sigma_{k_b}^2 &= \langle \delta u_2^2 \rangle = \sum_{n,n',j} M^{-1}_{2n} \left(\frac{\partial f_j}{\partial u_n} \right) M^{-1}_{2n'} \left(\frac{\partial f_j}{\partial u_{n'}} \right) \sigma_j^2
\end{aligned} \tag{34}$$

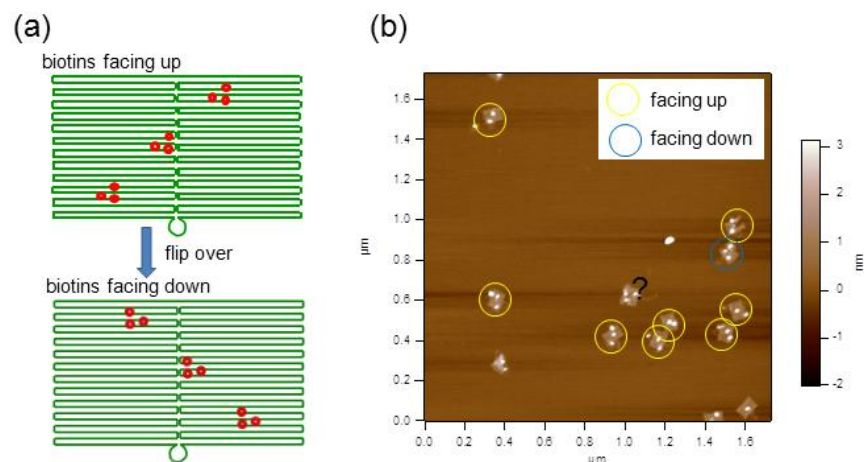


Figure S1. Analysis of DNA origami binding site orientation relative to substrate. (a) Illustration of chiral nature of DNA origami of Design II and (b) AFM image showing DNA origami with binding sites facing up and down. The bright spots on each origami are Qdots bound to it. The AFM images have been analyzed after Qdot binding because the small biotins themselves are not detectable by AFM. Analysis of multiple images indicates that the fraction of solution-facing binding sites is $> 90\%$.

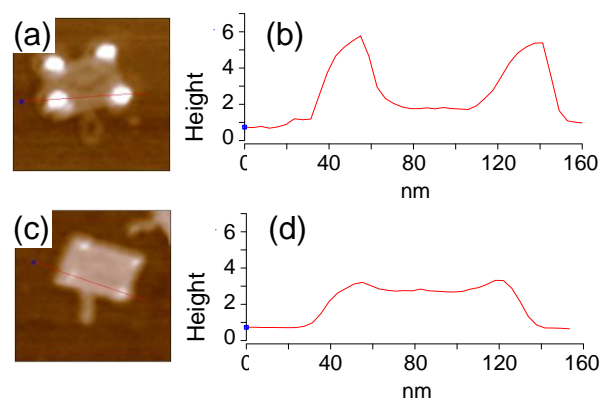


Figure S2. Cross-section analysis of AFM images for Design I. (a) AFM image and (b) corresponding cross-section analysis of quantum dot-DNA origami, (c) & (d) AFM image and corresponding section analysis of streptavidin-DNA origami.

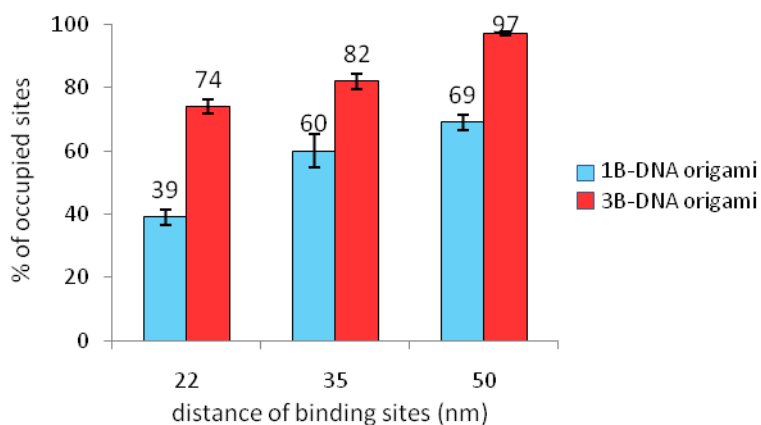


Figure S3. The binding yield of streptavidin coated quantum dot and 1B-DNA and 3B-DNA origami template (Design I). The percentage of occupied sites was calculated by counting the number of sites occupied by quantum dots and dividing it by the total number of available binding locations for each case. Data were collected on more than 240 origami pieces in AFM images for each case.

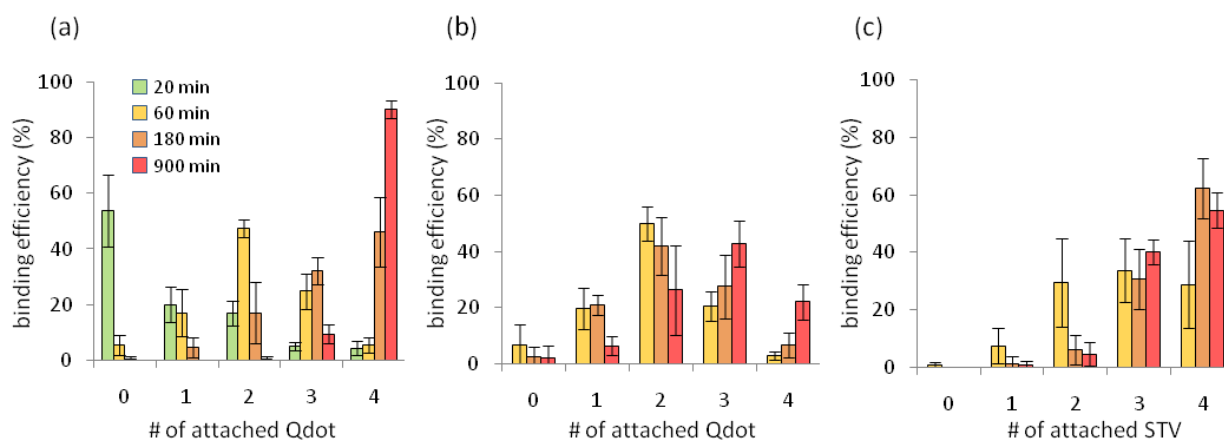


Figure S4. Product yield as a function of time (Design I, 50 nm spacing) for (a) 3B-DNA origami and (b) 1B-DNA origami. A control experiment was done with (c) streptavidin binding on 1B-DNA origami.

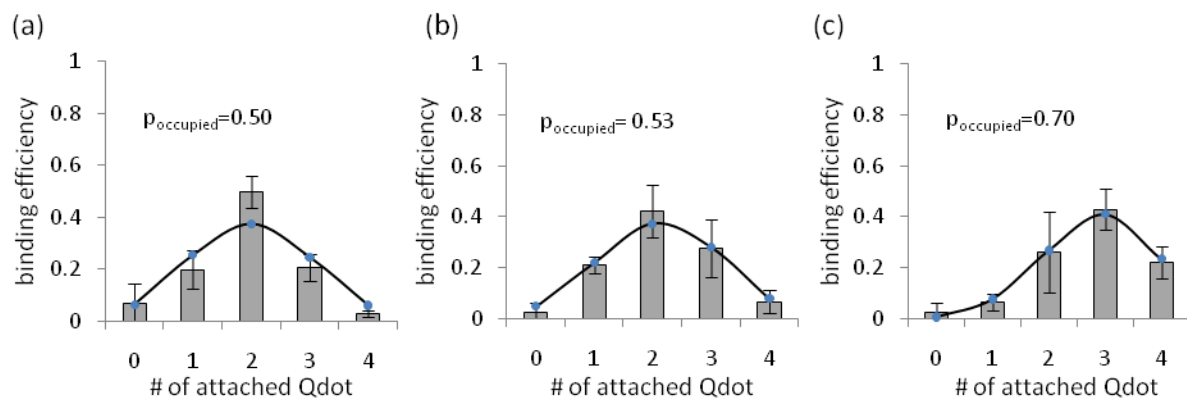


Figure S5. Histogram (bars) and calculated binomial distributions (line) of product yield on 1B-DNA origami of Design I (50nm spacing) as a function of reaction time. (a) 60 min, (b) 180 min, and (c) 900 min. The values of p_{occ} were calculated by doing a least squares fit of the data to a binomial distribution.

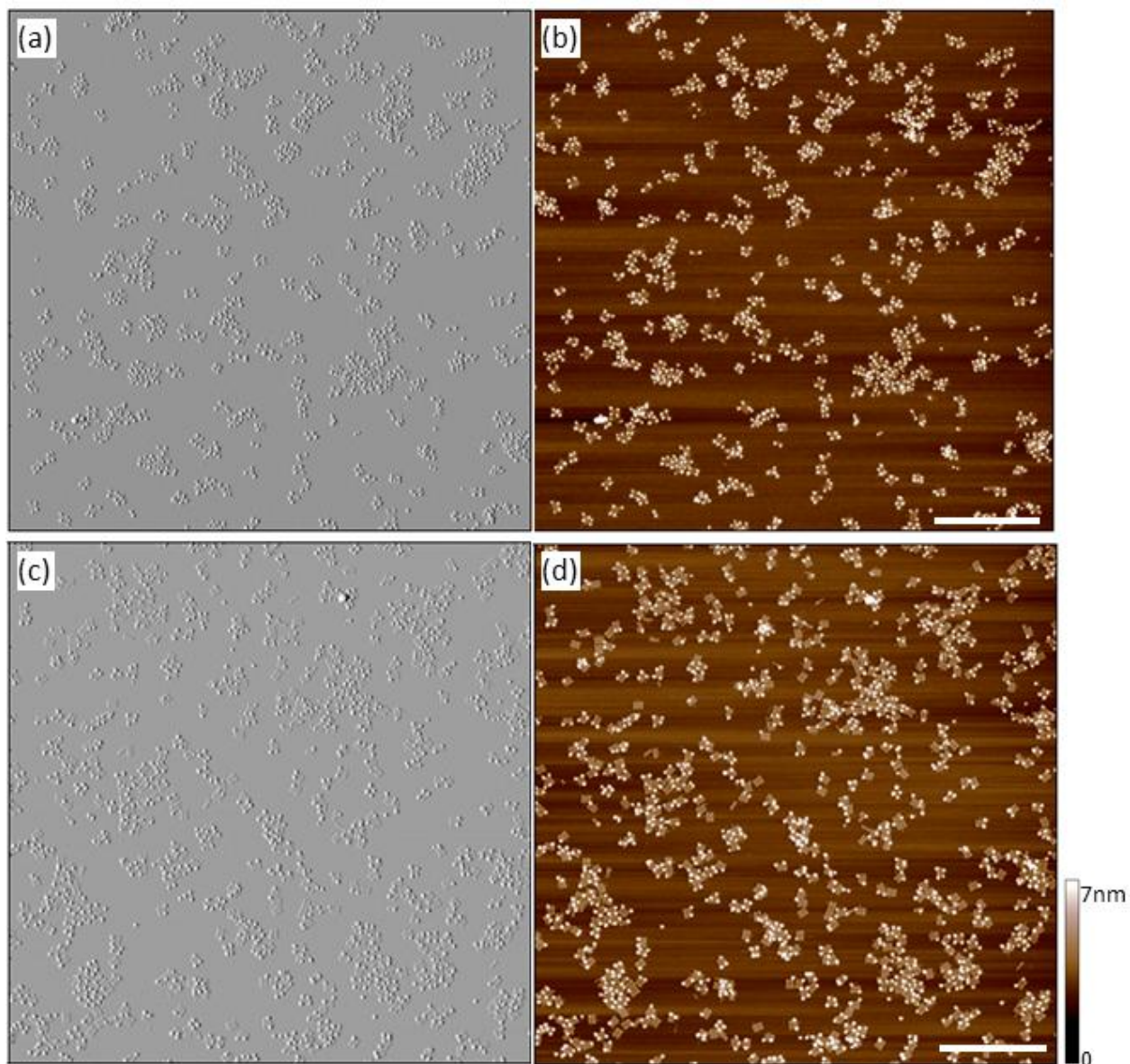


Figure S6. AFM images of amplitude mode (a & c) and corresponding height mode (b & d) for quantum dot nanopattern of Design I. (a), (b) on 3B-DNA origami and (c), (d) on 1B-DNA origami template. All Scale bars are 1 μm .

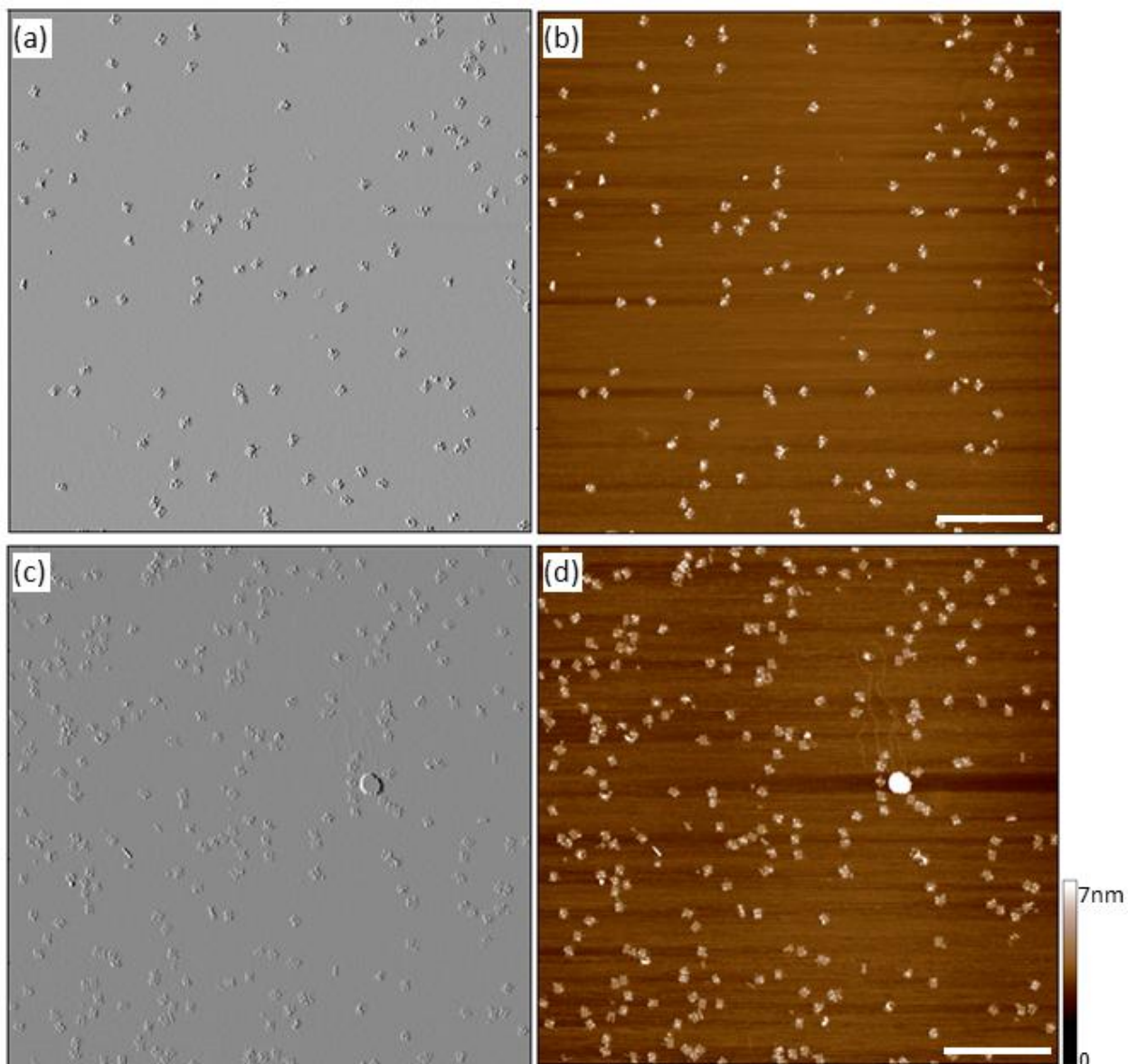


Figure S7. AFM images of amplitude mode (a & c) and corresponding height mode (b & d) for quantum dot nanopattern of Design II. (a), (b) on 3B-DNA origami and (c), (d) on 1B-DNA origami template. All Scale bars are 1 μm .

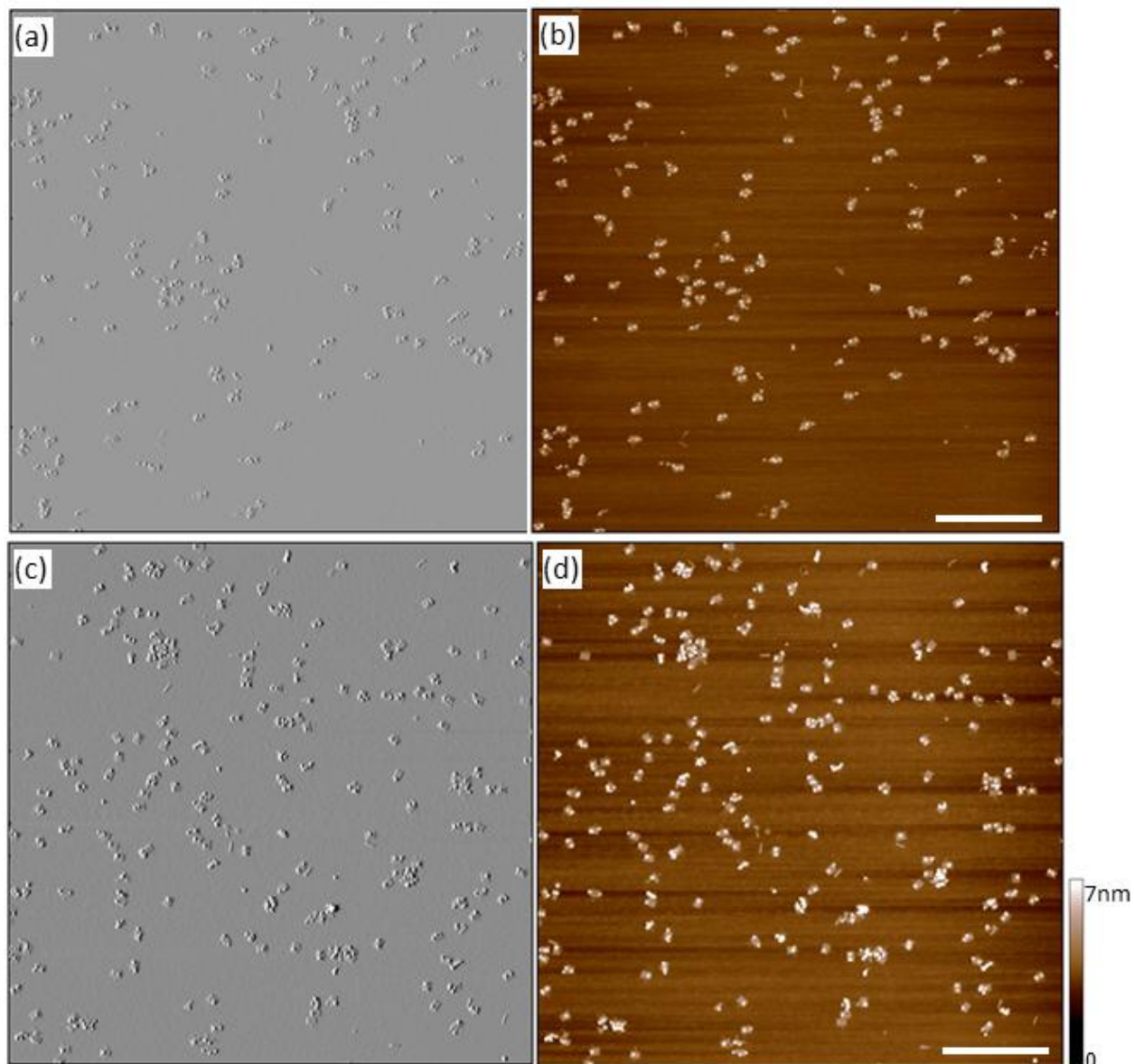


Figure S8. AFM images of amplitude mode (a & c) and corresponding height mode (b & d) for quantum dot nanopattern of Design III. (a), (b) on 3B-DNA origami and (c), (d) on 1B-DNA origami template. All Scale bars are 1 μm .

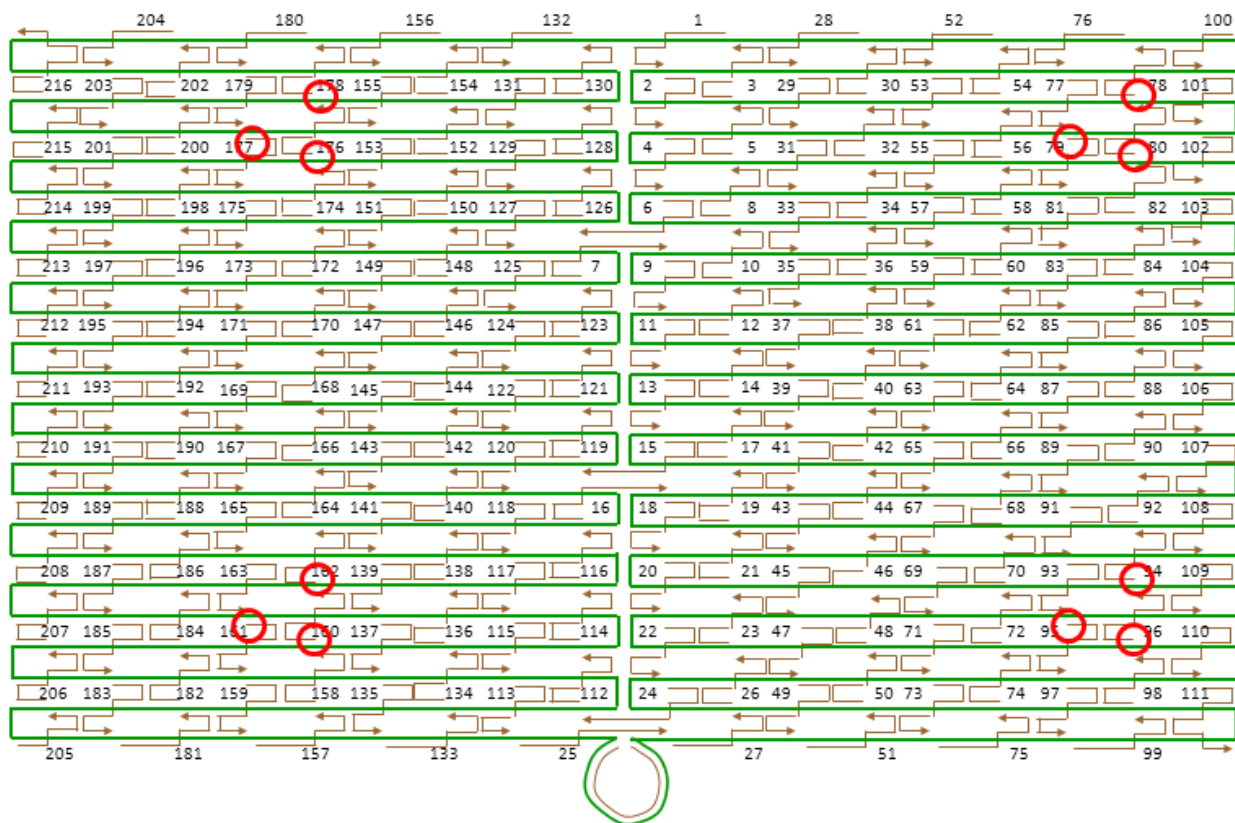


Figure S9. Schematic diagram of DNA origami template for Design I. M13mp18 single stranded DNA is light green; numbered staple strands are brown. The biotinylated staple strands are highlighted by red circles. The sequences of the staple strands and biotinylation information are listed and described in Table S2 and the following section.

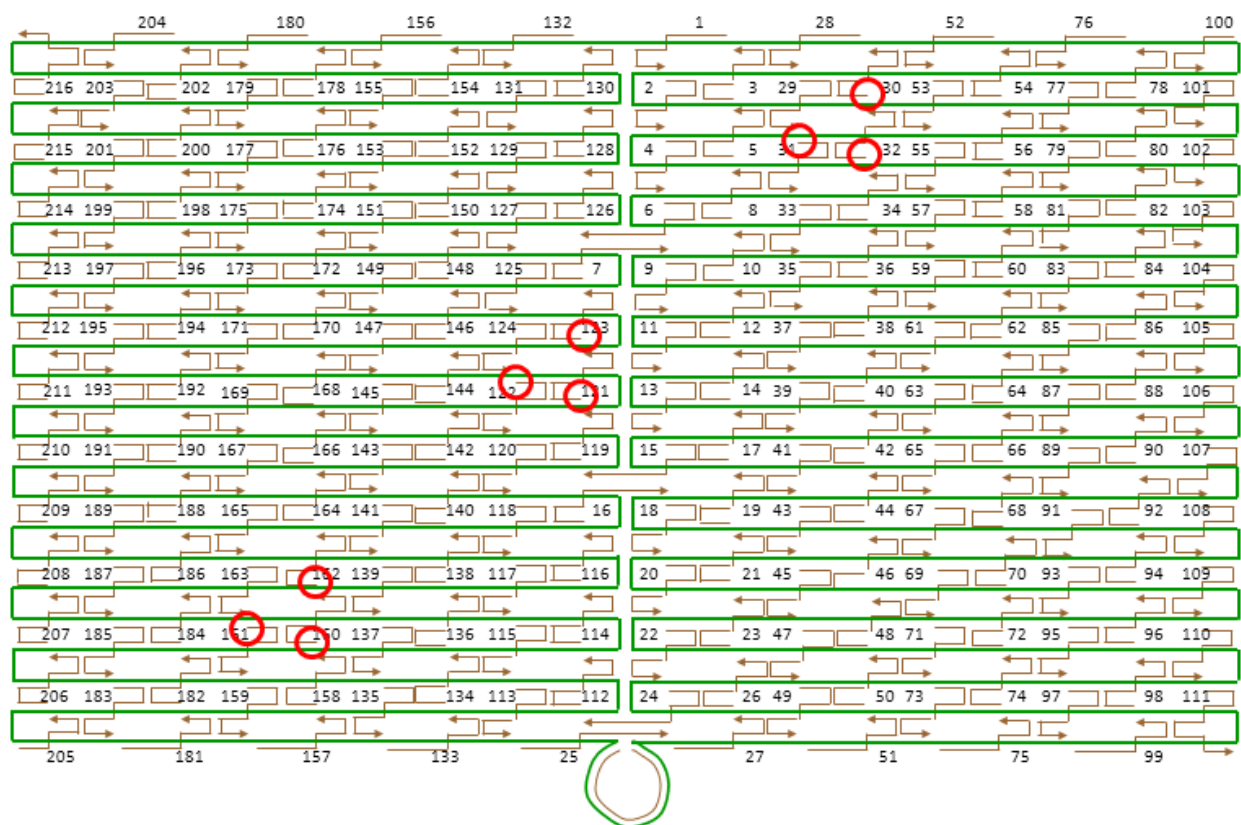


Figure S10. Schematic diagram of DNA origami template for Design II. M13mp18 single-stranded DNA is light green; numbered staple strands are brown. The biotinylated staple strands are highlighted by red circles. The sequences of the staple strands and biotinylation information are listed and described in Table S2 and the following section.

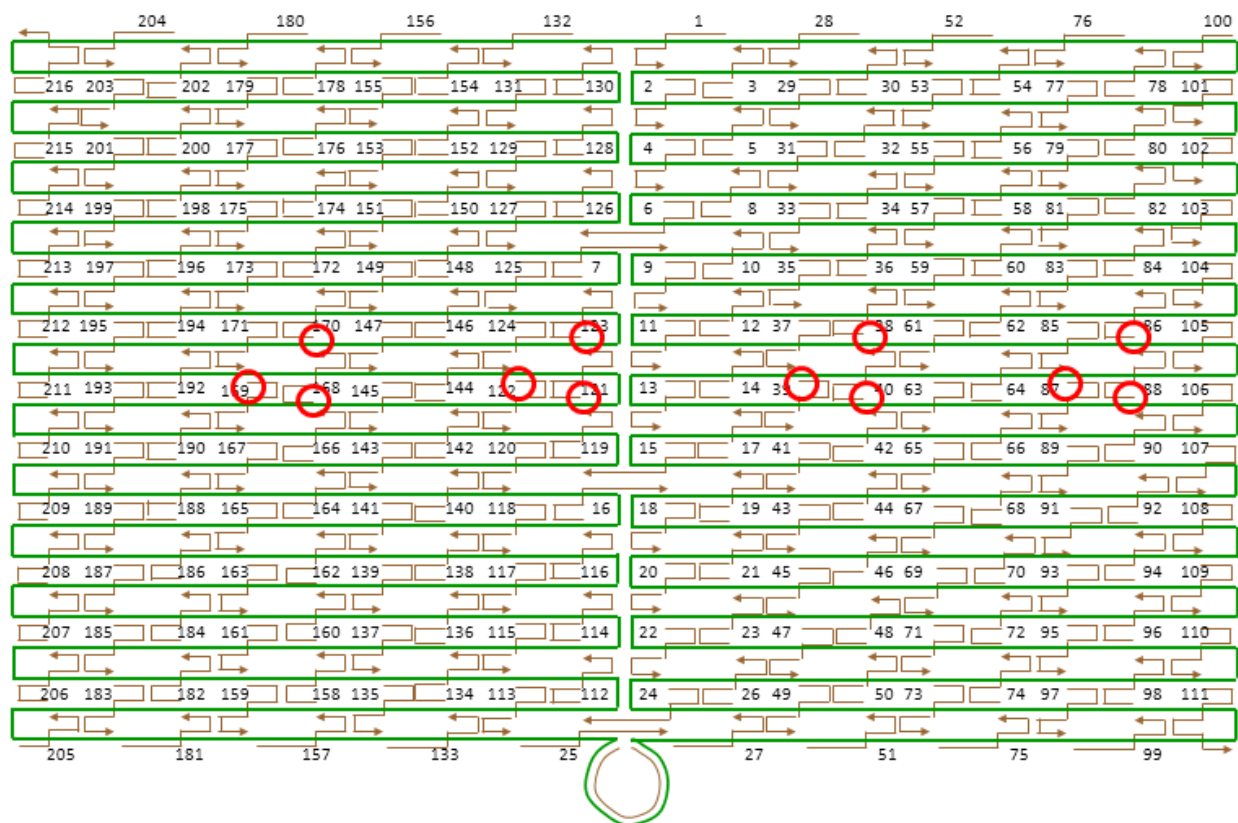


Figure S11. Schematic diagram of DNA origami template for Design III. M13mp18 single stranded DNA is light green; numbered staple strands are brown. The biotinylated staple strands are highlighted by red circles. The sequence of the staple strands and biotinylation information are listed and described in Table S2 and the following section.

Sequence of single-stranded M13mp18 can be found at the website of New England Biolab.
http://www.neb.com/nebecomm/tech_reference/restriction_enzyme/sequences/m13mp18.txt

Sequences of biotin-labeled staple strands

For preparing biotinylated DNA origami, specific staple strands were replaced by 5'-biotin labeled strands. The sequences of biotin labeled strands have the same sequences as the corresponding unmodified staple strands and have an extra spacer of thymines close to the 5'-biotin labeling. The following strands are for preparation of triple biotinylated DNA origami; underlined strands are for single biotinylated DNA origami preparation.

1. Design I
78, 79, 80, 94, 95, 96, 160, 161, 162, 176, 177, 178
2. Design II
30, 31, 32, 121, 122, 123, 160, 161, 162
3. Design III
38, 39, 40, 86, 87, 88, 121, 122, 123, 168, 169, 170

Table S2. Sequences of unmodified staple strands

Name	Sequence (5' → 3')
1	CAAGCCCAATAGGAAC CCATGTACAAACAGTT
2	AATGCCCGTAAACAGT GCCCGTATCTCCCTCA
3	TGCCTTGACTGCCTAT TTCGGAACAGGGATAG
4	GAGCCGCCCCACCACC GGAACCGCGACGGAAA
5	AACCAGAGACCCTCAG AACCGCCAGGGGTCAG
6	TTATTCATAGGGAAGG TAAATATT CATTCACT
7	CATAACCCGAGGCATA GTAAGAGC TTTTAAAG
8	ATTGAGGGTAAAGGTG AATTATCAATCACCGG
9	AAAAGTAATATCTTAC CGAAGCCCTTCCAGAG
10	GCAATAGCGCAGATAG CCGAACAATTCAACCG
11	CCTAATTTACGCTAAC GAGCGTCTAATCAATA
12	TCTTACCAGCCAGTTA CAAAATAAATGAAATA
13	ATCGGCTGCGAGCATG TAGAAACCTATCATAT
14	CTAATTTATCTTTCCT TATCATTATCCTGAA
15	GCGTTATAGAAAAAGC CTGTTTAG AAGGCCGG
16	GCTCATTTTCGCATTA AATTTTGT AGCTTAGA
17	AATTACTACAAATTCT TACCAGTAATCCCATC
18	TTAAGACGTTGAAAAC ATAGCGATAACAGTAC
19	TAGAATCCCTGAGAAG AGTCAATAGGAATCAT
20	CTTTTACACAGATGAA TATACAGTAAACAATT
21	TTTAACGTTTCGGGAGA AACAATAATTTTCCCT
22	CGACAATAAGTATTA GACTTTACAATACCGA
23	GGATTTAGCGTATTA ATCCTTTGTTTTCAGG
24	ACGAACCAAAACATCG CCATTAAA TGGTGGTT

25	GAACGTGGCGAGAAAG GAAGGGAA CAAACTAT
26	TAGCCCTACCAGCAGA AGATAAAAACATTTGA
27	CGGCCTTGCTGGTAAT ATCCAGAACGAACTGA
28	CTCAGAGCCACCACCC TCATTTTCCTATTATT
29	CTGAAACAGGTAATAA GTTTTAACCCCTCAGA
30	AGTGTACTTGAAAGTA TTAAGAGGCCGCCACC
31	GCCACCCTCTTTTCA TAATCAAACCGTCACC
32	GTTTGCCACCTCAGAG CCGCCACCGATACAGG
33	GACTTGAGAGACAAAA GGGCGACAAGTTACCA
34	AGCGCCAACCATTTGG GAATTAGATTATTAGC
35	GAAGGAAAATAAGAGC AAGAAACAACAGCCAT
36	GCCCAATACCGAGGAA ACGCAATAGGTTTACC
37	ATTATTTAACCCAGCT ACAATTTTCAAGAACG
38	TATTTTGCTCCCAATC CAAATAAGTGAGTTAA
39	GGTATTAAGAACAAGA AAAATAATTAAGCCA
40	TAAGTCCTACCAAGTA CCGCACTCTTAGTTGC
41	ACGCTCAAATAAGAA TAAACACCGTGAATTT
42	AGGCGTTACAGTAGGG CTTAATTGACAATAGA
43	ATCAAAATCGTCGCTA TTAATTAACGGATTCCG
44	CTGTAAATCATAGGTC TGAGAGACGATAAATA
45	CCTGATTGAAAGAAAT TGCGTAGACCCGAACG
46	ACAGAAATCTTTGAAT ACCAAGTTCCTTGCTT
47	TTATTAATGCCGTCAA TAGATAATCAGAGGTG
48	AGATTAGATTTAAAAG TTTGAGTACACGTAAA
49	AGGCGGTCATTAGTCT TTAATGCGCAATATTA
50	GAATGGCTAGTATTAA CACCGCCTCAACTAAT
51	CCGCCAGCCATTGCAA CAGGAAAAATATTTTT
52	CCCTCAGAACCGCCAC CCTCAGAACTGAGACT
53	CCTCAAGAATACATGG CTTTTGATAGAACCAC
54	TAAGCGTCGAAGGATT AGGATTAGTACCGCCA
55	CACCAGAGTTCGGTCA TAGCCCCCGCCAGCAA
56	TCGGCATTCCGCCGCC AGCATTGACGTTCCAG
57	AATCACCAATAGAAA ATTCATATATAACGGA
58	TCACAATCGTAGCACC ATTACCATCGTTTTCA
59	ATACCCAAGATAACCC ACAAGAATAAACGATT
60	ATCAGAGAAAGAACTG GCATGATTTTATTTTG
61	TTTTGTTAAGCCTTA AATCAAGAATCGAGAA
62	AGGTTTTGAACGTCAA AAATGAAAGCGCTAAT
63	CAAGCAAGACGCGCCT GTTTATCAAGAATCGC
64	AATGCAGACCGTTTTT ATTTTCATCTTGCGGG
65	CATATTTAGAAATACC GACCGTGTTACCTTTT
66	AATGGTTTACAACGCC AACATGTAGTTCAGCT
67	TAACCTCCATATGTGA GTGAATAAACAAAATC
68	AAATCAATGGCTTAGG TTGGGTTACTAAATTT
69	GCGCAGAGATATCAAA ATTATTTGACATTATC
70	AACCTACCGCGAATTA TTCATTTCCAGTACAT
71	ATTTTGCGTCTTTAGG AGCACTAAGCAACAGT

72	CTAAAATAGAACAAAG AAACCACCAGGGTTAG
73	GCCACGCTATACGTGG CACAGACAACGCTCAT
74	GCGTAAGAGAGAGCCA GCAGCAAAAAGGTTAT
75	GGAAATACCTACATTT TGACGCTCACCTGAAA
76	TATCACCGTACTCAGG AGGTTTAGCGGGGTTT
77	TGCTCAGTCAGTCTCT GAATTTACCAGGAGGT
78	GGAAAGCGACCAGGCG GATAAGTGAATAGGTG
79	TGAGGCAGGCGTCAGA CTGTAGCGTAGCAAGG
80	TGCCTTTAGTCAGACG ATTGGCCTGCCAGAAT
81	CCGGAAACACACCACG GAATAAGTAAGACTCC
82	ACGCAAAGGTCACCAA TGAAACCAATCAAGTT
83	TTATTACGGTCAGAGG GTAATTGAATAGCAGC
84	TGAACAAACAGTATGT TAGCAAATAAAAGAA
85	CTTTACAGTTAGCGAA CCTCCCGACGTAGGAA
86	GAGGCGTTAGAGAATA ACATAAAAGAACACCC
87	TCATTACCCGACAATA AACACATATTTAGGC
88	CCAGACGAGCGCCCAA TAGCAAGCAAGAACGC
89	AGAGGCATAATTCAT CTTCTGACTATAACTA
90	TTTTAGTTTTTCGAGC CAGTAATAAATTCTGT
91	TATGTAAACCTTTTTT AATGGAAAAATTACCT
92	TTGAATTATGCTGATG CAAATCCACAAATATA
93	GAGCAAAAACCTTCTGA ATAATGGAAGAAGGAG
94	TGGATTATGAAGATGA TGAACAAAATTTTCAT
95	CGGAATTATTGAAAGG AATTGAGGTGAAAAAT
96	ATCAACAGTCATCATA TTCCTGATTGATTGTT
97	CTAAAGCAAGATAGAA CCCTTCTGAATCGTCT
98	GCCAACAGTCACCTTG CTGAACCTGTTGGCAA
99	GAAATGGATTATTTAC ATTGGCAGACATTCTG
100	TTTT TATAAGTA TAGCCCGGCCGTCGAG
101	AGGGTTGA TTTT ATAAATCC TCATTAATGATATTC
102	ACAAACAA TTTT AATCAGTA GCGACAGATCGATAGC
103	AGCACCGT TTTT TAAAGGTG GCAACATAGTAGAAAA
104	TACATACA TTTT GACGGGAG AATTAACACAGGGAA
105	GCGCATT TTTT GCTTATCC GGTATTCTAAATCAGA
106	TATAGAAG TTTT CGACAAA GGTAAAGTAGAGAATA
107	TAAAGTAC TTTT CGCGAGAA AACTTTTTATCGCAAG
108	ACAAAGAA TTTT ATTAATTA CATTTAACACATCAAG
109	AAAACAAA TTTT TTCATCAA TATAATCCTATCAGAT
110	GATGGCAA TTTT AATCAATA TCTGGTCACAAATATC
111	AAACCCTC TTTT ACCAGTAA TAAAAGGGATTCACCA GTCACACGTTTT
112	CCGAAATCCGAAAATC CTGTTTGAAGCCGGAA
113	CCAGCAGGGGCAAAAT CCCTTATAAAGCCGGC
114	GCATAAAGTTCCACAC AACATACGAAGCGCCA
115	GCTCACAATGTAAAGC CTGGGGTGGGTTTGCC
116	TTCCGCAATTGCCGGAA ACCAGGCATTAATCA
117	GCTTCTGGTCAGGCTG CGCAACTGTGTTATCC
118	GTAAAAATTTTAACCA ATAGGAACCCGGCACC

119	AGACAGTCATTCAAAA GGGTGAGAAGCTATAT
120	AGGTAAGAAATCACC ATCAATATAATATTTT
121	TTTCATTTGGTCAATA ACCTGTTTATATCGCG
122	TCGCAAATGGGGCGCG AGCTGAAATAATGTGT
123	TTTTAATTGCCCGAAA GACTTCAAAACACTAT
124	AAGAGGAACGAGCTTC AAAGCGAAGATACATT
125	GGAATTACTCGTTTAC CAGACGACAAAAGATT
126	GAATAAGGACGTAACA AAGCTGCTCTAAAACA
127	CCAAATCACTTGCCCT GACGAGAACGCCAAAA
128	CTCATCTTGAGGCAAA AGAATACAGTGAATTT
129	AAACGAAATGACCCCC AGCGATTATTCATTAC
130	CTTAAACATCAGCTTG CTTTCGAGCGTAACAC
131	TCGGTTTAGCTTGATA CCGATAGTCCAACCTA
132	TGAGTTTCGTCACCAG TACAACTTAATTGTA
133	CCCCGATTTAGAGCTT GACGGGGAAATCAAAA
134	GAATAGCCGCAAGCGG TCCACGCTCCTAATGA
135	GAGTTGCACGAGATAG GGTTGAGTAAGGGAGC
136	GTGAGCTAGTTTCCTG TGTGAAATTTGGGAAG
137	TCATAGCTACTCACAT TAATTGCGCCCTGAGA
138	GGCGATCGCACTCCAG CCAGCTTTGCCATCAA
139	GAAGATCGGTGCGGGC CTCTTCGCAATCATGG
140	AAATAATTTTAAATTG TAAACGTTGATATTCA
141	GCAAATATCGCGTCTG GCCTTCCTGGCCTCAG
142	ACCGTTCTAAATGCAA TGCCTGAGAGGTGGCA
143	TATATTTTAGCTGATA AATTAATGTTGTATAA
144	TCAATTCTTTTAGTTT GACCATTACCAGACCG
145	CGAGTAGAACTAATAG TAGTAGCAAACCCTCA
146	GAAGCAAAAAGCGGA TTGCATCAGATAAAAA
147	TCAGAAGCCTCCAACA GGTCAGGATCTGCGAA
148	CCAAAATATAATGCAG ATACATAAACACCAGA
149	CATTCAACGCGAGAGG CTTTTGCATATTATAG
150	ACGAGTAGTGACAAGA ACCGGATATACCAAGC
151	AGTAATCTTAAATTGG GCTTGAGAGAATACCA
152	GCGAAACATGCCACTA CGAAGGCATGCGCCGA
153	ATACGTAAAAGTACAA CGGAGATTTTCATCAAG
154	CAATGACACTCCAAAA GGAGCCTTACAACGCC
155	AAAAAAGGACAACCAT CGCCCACGCGGGTAAA
156	TGTAGCATTCCACAGA CAGCCCTCATCTCCAA
157	GTAAAGCACTAAATCG GAACCCTAGTTGTTCC
158	AGTTTGGAGCCCTTCA CCGCCTGGTTGCGCTC
159	AGCTGATTACAAGAGT CCACTATTGAGGTGCC
160	ACTGCCCGCCGAGCTC GAATTCGTTATTACGC
161	CCCGGGTACTTTCCAG TCGGGAAACGGGCAAC
162	CAGCTGGCGGACGACG ACAGTATCGTAGCCAG
163	GTTTGAGGGAAAGGGG GATGTGCTAGAGGATC
164	CTTTCATCCCCAAAAA CAGGAAGACCGGAGAG
165	AGAAAAGCAACATTAA ATGTGAGCATCTGCCA

166	GGTAGCTAGGATAAAA ATTTTTAGTTAACATC
167	CAACGCAATTTTTGAG AGATCTACTGATAATC
168	CAATAAATACAGTTGA TTCCAATTTAGAGAG
169	TCCATATACATACAGG CAAGGCAACTTTATTT
170	TACCTTTAAGGTCTTT ACCCTGACAAAGAAGT
171	CAAAAATCATTGCTCC TTTTGATAAGTTTCAT
172	TTTGCCAGATCAGTTG AGATTTAGTGGTTTAA
173	AAAGATTCAGGGGGTA ATAGTAAACCATAAAT
174	TTTCAACTATAGGCTG GCTGACCTTGTATCAT
175	CCAGGCGCTTAATCAT TGTGAATTACAGGTAG
176	CGCCTGATGGAAGTTT CCATTAAACATAACCG
177	TTTCATGAAAATTGTG TCGAAATCTGTACAGA
178	ATATATTCTTTTTTCA CGTTGAAAATAGTTAG
179	AATAATAAGGTGCGCTG AGGCTTGCAAAGACTT
180	CGTAACGATCTAAAGT TTTGTGCGTGAATTGCG
181	ACCCAAATCAAGTTTT TTGGGGTCAAAGAACG
182	TGGACTCCCTTTTCCAC CAGTGAGACCTGTCGT
183	TGGTTTTTAACGTCAA AGGGCGAAGAACCATC
184	GCCAGCTGCCTGCAGG TCGACTCTGCAAGGCG
185	CTTGCATGCATTAATG AATCGGCCCGCCAGGG
186	ATTAAGTTCGCATCGT AACCGTGCGAGTAACA
187	TAGATGGGGGGTAACG CCAGGGTTGTGCCAAG
188	ACCCGTGTCATATGT ACCCCGGTAAAGGCTA
189	CATGTCAAGATTCTCC GTGGGAACCGTTGGTG
190	TCAGGTCACTTTTGCG GGAGAAGCAGAATTAG
191	CTGTAATATTGCCTGA GAGTCTGAAAACACTAG
192	CAAAATTAAGTACGG TGTCTGGAAGAGGTCA
193	TGCAACTAAGCAATAA AGCCTCAGTTATGACC
194	TTTTTGCGCAGAAAAC GAGAATGAATGTTTAG
195	AAACAGTTGATGGCTT AGAGCTTATTTAAATA
196	ACTGGATAACGGAACA ACATTATTACCTTATG
197	ACGAACTAGCGTCCAA TACTGCGGAATGCTTT
198	CGATTTTAGAGGACAG ATGAACGGCGCGACCT
199	CTTTGAAAAGAAGTGG CTCATTATTTAATAAA
200	GCTCCATGAGAGGCTT TGAGGACTAGGGAGTT
201	ACGGCTACTTACTTAG CCGGAACGCTGACCAA
202	AAAGGCCGAAAGGAAC AACTAAAGCTTTCCAG
203	GAGAATAGCTTTTGCG GGATCGTCCGGTAGCA
204	ACGTTAGTAAATGAAT TTTCTGTAAGCGGAGT
205	TTTT CGATGGCC CACTACGTAAACCGTC
206	TATCAGGG TTTT CGGTTTGC GTATTGGGAACGCGCG
207	GGGAGAGG TTTT TGTA AAC GACGGCCATTCCCAGT
208	CACGACGT TTTT GTAATGGG ATAGGTCAAACGGCG
209	GATTGACC TTTT GATGAACG GTAATCGTAGCAAACA
210	AGAGAATC TTTT GGTTGTAC CAAAACAAGCATAAA
211	GCTAAATC TTTT CTGTAGCT CAACATGTATTGCTGA
212	ATATAATG TTTT CATTGAAT CCCCTCAAATCGTCA

213	TAAATATT TTTT GGAAGAAA AATCTACGACCAGTCA
214	GGACGTTG TTTT TCATAAGG GAACCGAAAGGCGCAG
215	ACGGTCAA TTTT GACAGCAT CGGAACGAACCCTCAG
216	CAGCGAAAA TTTT ACTTTCA ACAGTTTCTGGGATTT TGCTAAAC TTTT
Loop1	AACATCACTTGCCTGAGTAGAAGAACT
Loop2	TGTAGCAATACTTCTTTGATTAGTAAT
Loop3	AGTCTGTCCATCACGCAAATTAACCGT
Loop4	ATAATCAGTGAGGCCACCGAGTAAAAG
Loop5	ACGCCAGAATCCTGAGAAGTGTTTTT
Loop6	TTAAAGGGATTTTAGACAGGAACGGT
Loop7	AGAGCGGGAGCTAAACAGGAGGCCGA
Loop8	TATAACGTGCTTTCCTCGTTAGAATC
Loop9	GTAATATGGTTGCTTTGACGAGCACG
Loop10	GCGCTTAATGCGCCGCTACAGGGCGC